	ESA Climate Change Initiative (CCI+)	Page 1
	Climate Assessment Report (CAR) for Climate Research Data Package 7 (CRDP#7)	
	of the Essential Climate Variable (ECV) Greenhouse Gases (GHG)	Version 1.1
		20 March 2023

ESA Climate Change Initiative (CCI+)

Climate Assessment Report (CAR)

for Climate Research Data Package No. 7 (CRDP#7)

of the Essential Climate Variable (ECV)


Greenhouse Gases (GHG)

Project: GHG-CCI+

Frédéric Chevallier^a and Julia Marshall^b

^a Laboratoire des Sciences du Climat et de l'Environnement (LSCE), Gif-sur-Yvette, France

^b Institut für Physik der Atmosphäre, Deutsches Zentrum für Luft- und Raumfahrt (DLR), Oberpfaffenhofen, Germany

	ESA Climate Change Initiative (CCI+) Climate Assessment Report (CAR) for Climate Research Data Package 7 (CRDP#7) of the Essential Climate Variable (ECV) Greenhouse Gases (GHG)	Page 2
		Version 1.1
		20 March 2023

Change log:

Version Nr.	Date	Status	Reason for change
Version 0.0	17 February 2022	Initial draft	User assessment for CRDP#7 XCO ₂ products
Version 1.0	10 March 2023	Final draft	User assessment for CRDP#7 XCH ₄ products added
Version 1.1	20 March 2023	As submitted	Minor editorial changes at various places

This document should be cited as:

Chevallier, F. and Marshall, J., Climate Assessment Report for Climate Research Data Package No. 7 (CRDP#7) of ESA's Climate Change Initiative project GHG-CCI+, version 1.1, 20 March 2023, 2023.



	ESA Climate Change Initiative (CCI+) Climate Assessment Report (CAR) for Climate Research Data Package 7 (CRDP#7) of the Essential Climate Variable (ECV) Greenhouse Gases (GHG)	Page 3
		Version 1.1
		20 March 2023

Table of contents

1. Executive summary.....	4
2. User related aspects discussed in the peer-reviewed literature	9
3. Assessment of satellite-derived XCO₂ products	13
3.1. Introduction	13
3.2. Comparisons with forward model simulations	14
3.2.1. Method.....	14
3.2.2. Results	14
3.3. Inversion experiments with the LSCE system	16
3.3.1. Method.....	16
3.3.2. Global annual atmospheric growth rates	17
3.3.3. Maps of annual budgets	18
3.3.4. Annual budget time series.....	20
3.3.5. Conclusions	21
4. Assessment of satellite-derived XCH₄ data products	22
4.1. Introduction	22
4.2. Comparisons with forward model simulations	24
4.2.1. Method.....	24
4.2.2. Results	25
4.2.2.1. Overview of measurement coverage	25
4.2.2.2. Bias-correction based on surface-optimized fields	28
4.3. Methane inversion experiments with the Jena CarboScope	29
4.3.1. Method.....	29
4.3.2. Global mean atmospheric mixing ratio and growth rate	30
4.3.3. Maps of annual budgets	31
4.3.4. Year-on-year flux increments	33
4.3.5. Comparison with aircraft data and TCCON	34
4.3.6. Conclusions	36
Acknowledgements	37
References.....	38

	ESA Climate Change Initiative (CCI+) Climate Assessment Report (CAR) for Climate Research Data Package 7 (CRDP#7) of the Essential Climate Variable (ECV) Greenhouse Gases (GHG)	Page 4
		Version 1.1
		20 March 2023

1. Executive summary

This report describes the **assessment of the Essential Climate Variable (ECV) data products of the seventh release of the GHG-CCI Climate Research Data Package (CRDP#7)** by the Climate Research Group (CRG) of the GHG-CCI+ project (Buchwitz et al. 2015, 2017; see also GHG-CCI+ website <https://climate.esa.int/en/projects/ghgs/>). These products are CO₂ and CH₄ column retrievals (XCO₂ and XCH₄) from current satellite instruments:

- **CO2_OC2_FOCA:** XCO₂ from NASA's OCO-2 satellite retrieved by University of Bremen using the FOCAL algorithm (global, Sep. 2014 – March 2021, v10)
- **CO2_TAN_OCFP:** XCO₂ from China's TanSat satellite retrieved by University of Leicester using the UoL-FP (or OCFP) algorithm (global lands, March 2017 – April 2018, v1.2)
- XCO₂ and XCH₄ from Japan's GOSAT-2 satellite (products **CO2_GO2_SRFP**, **CH4_GO2_SRFP**, **CH4_GO2_SRPR**, global, Feb. 2019 – August 2020, v2.0.0)
- **CH4_S5P_WFMD:** XCH₄ from the European Sentinel-5-Precursor (S5P) satellite retrieved by University of Bremen using the WFM-DOAS algorithm (global, Nov. 2017 – Dec. 2020, v1.5)


These products are available via the CCI Open Data Portal (<https://climate.esa.int/en/odp/#/dashboard>).

Climate researchers may find interest in these products for various reasons like evaluating climate models, estimating the uncertain parameters of these climate models, studying the variability of CO₂ and CH₄ in the atmosphere, studying wildfire or fossil fuel emission plumes, or quantifying the surface fluxes of these gases.

CRDP#7 is the third release of products from the GHG-CCI+ project, which started in March 2019.

Datasets CRDP#1 to CRDP#4 have been generated and released by the GHG-CCI pre-cursor project (2010 - 2018). These products are CO₂ and CH₄ products from SCIAMACHY/ENVISAT, MIPAS/ENVISAT, GOSAT, AIRS and IASI. The XCO₂ and XCH₄ and IASI products are now generated operationally via the Copernicus Climate Change Service (C3S, <https://climate.copernicus.eu/>) and are available via the Copernicus Climate Data Store (CDS, <https://cds.climate.copernicus.eu/>).

By producing retrievals of the CO₂ and CH₄ columns for these satellites and others, CRDP has given a **unique**, though heterogeneous, **climate record from space covering now more than fifteen years** of the two major greenhouse gases of anthropogenic origin. **This length opens the possibility to characterize emission trends, as was already demonstrated by a series of CRDP-based studies for CH₄** (Bergamaschi et al. 2013) **and for CO₂** (Ross et al. 2013, Schneising et al. 2013a, 2013b, Reuter et al. 2014b, Detmers et al. 2015). For the entire publication list please see <https://climate.esa.int/en/projects/ghgs/publications/>.

	ESA Climate Change Initiative (CCI+) Climate Assessment Report (CAR) for Climate Research Data Package 7 (CRDP#7) of the Essential Climate Variable (ECV) Greenhouse Gases (GHG)	Page 5
		Version 1.1
		20 March 2023

Previous iterations of the CRDP explored an ensemble-based approach to make use of the range of retrieval product covering several sensors and multiple retrieval algorithms (EMMA). **This ensemble approach allowed for a more comprehensive assessment of the product uncertainty than just the typical uncertainty characterisation of each product through internal uncertainty propagation.**


Reuter et al. (2013, 2014a, 2020) illustrated this capability well.

The CRDP data sets, together with satellite retrievals made outside Europe, has already served to **quantify regional carbon budgets** (e.g., Basu et al. 2013, Bergamaschi et al. 2013, Fraser et al. 2013, Monteil et al. 2013, Cressot et al. 2013) and more specifically (for CO₂) Canada and Siberian forests (Schneising et al. 2011), Eurasia (Guerlet et al. 2013a), Tropical Asia (Basu et al. 2014), Amazonia (Parazoo et al. 2013) and Europe (Reuter et al. 2014a). However, for CO₂, there remains considerable discrepancies with bottom up estimates or inversions based on atmospheric in-situ observations (Chevallier et al. 2014a, 2019, Feng et al. 2016a, Reuter et al. 2016c). These discrepancies were also highlighted in the first six releases of the CAR (Chevallier et al. 2013, 2015, 2016, 2017; Chevallier 2020; Chevallier and Marshall 2021). For CH₄ it has been clearly demonstrated that the SCIAMACHY retrievals and the GOSAT retrievals provide important information on regional methane emissions (e.g., Bergamaschi et al. 2013, Fraser et al. 2013, Alexe et al. 2015).

Each application of the CRDP has specific user requirements (e.g., Chevallier et al., 2014b) and it is not possible to exhaustively cover them in the CRG. Instead, the CRG has focussed on global source-sink inversion from several viewpoints.

For CO₂, this study has covered the three XCO₂ products of CRDP#7: CO2_OC2_FOCA which has been retrieved from OCO-2 over both land and ocean, CO2_TAN_OCFP which has been retrieved over land from TanSat and CO2_GO2_SRFP which has been retrieved from GOSAT-2 over both land and ocean. The starting point of this report is the comparison between these products and the independent CAMS v20r2 transport model simulation (with surface fluxes inferred through inversion of high precision measurements of atmospheric CO₂ in situ samples). The satellite retrievals fit the independent CAMS simulation over land and ocean at the RMS level of 1 to 3 ppm, depending on the product, the latitude and the geotype. Improved statistics were obtained when comparing NASA's ACOS OCO-2 retrievals, version 10, with the CAMS simulation over land as over ocean. This tends to confirm that the individual ACOS retrievals have better precision than the CRDP#7 ones, as already reported in the uncertainty variable of the respective retrieval data files.

The assimilation of the CRDP#7 products in the LSCE global inversion system infers CO₂ surface fluxes that are very different from those obtained by both the assimilation of surface air-sample measurements and the assimilation of NASA's retrievals from OCO-2. We think that they are less credible on the basis of current knowledge of the carbon cycle. We particularly highlighted the atmospheric growth rate and the location of the ocean outgassing regions. We related these features to the relatively large RMS differences of the CRDP#7 products to the CAMS reference surface air-sample inversion, in particular for CO2_GO2_SRFP. We note a small improvement of the growth rate inferred by assimilating CO2_OC2_FOCA from CRDP#6 to CRDP#7 versions. The consistent results

	ESA Climate Change Initiative (CCI+) Climate Assessment Report (CAR) for Climate Research Data Package 7 (CRDP#7) of the Essential Climate Variable (ECV) Greenhouse Gases (GHG)	Page 6
		Version 1.1
		20 March 2023

obtained in the inversion between the surface air-sample measurements and the ACOS retrievals demonstrates that there is no fundamental limitation in atmospheric inverse modelling (e.g., in the realism of the transport model or in the modelled error statistics) when assimilating satellite XCO₂ retrievals. The ACOS-driven CO₂ surface fluxes have actually been part of the official CAMS data portfolio since year 2019.


ACOS and CO2_OC2_FOCA exploit the same OCO-2 spectra. The various tests performed do not allow us to identify the distinctive asset of ACOS in our system, but the dramatic increase in the CO2_OC2_FOCA data volume since CRDP#6 now excludes a too low data density. The following hypotheses remain: the data precision, the data trueness (linked both to the quality of the physical retrieval scheme and to its empirical bias-correction), the accuracy of the auxiliary data (averaging kernels), or a combination of these qualities at once. These hypotheses implicitly involve the retrieval quality control. Detailed sensitivity tests could be performed for this.

CO2_OC2_FOCA's distinct advantage compared to ACOS is its representation of multiple scattering effects in the radiative transfer in a form that is not costlier than absorption. In preparation for the Copernicus CO₂ Monitoring Mission that will provide even larger amount of data than OCO-2 (Pinty et al., 2017), CO2_OC2_FOCA represents an important achievement. To a smaller extent (in terms of data volume), the same can be said of CO2_TAN_OCFP. In this context and resources permitting, it would be important to document their performance in more detail in order to help prioritize future developments.

For CH₄, product CH4_S5P_WFMD, using TROPOMI measurements from S5P, is not the only data product that covers multiple years. In order to expand the scope of this assessment, the operational S5P retrieval using the RemoTeC algorithm (hereafter referred to as CH4_S5P_SRON) has been included in the assessment, as well as the pre-operational RemoTeC product based on Lorente et al. (2021), referred to as CH4_S5P_SRONt. Furthermore, some initial comparison of the GOSAT-2 retrievals (CH4_GO2_SRFP and CH4_GO2_SRPR) have been included as well. When the related assessments have been carried out, these retrievals were only available for 18 months, but a first assessment of the products was carried out.

The comparison begins by comparing the XCH₄ products to an inversion optimized using measurements from 31 flask measurement sites around the world. This is a rather limited dataset, but it is what is available over the time period in question. In general, satellite retrievals are available for use with much less lag time than are contemporaneous in-situ measurements, which is a limitation when assessing retrievals less than a year after the measurement time.

The comparison of the surface-optimized concentration fields with the satellite products shows a systematic offset with a latitudinal dependence. This is likely largely due to errors in the transport model due to poorly represented tropopause height and stratospheric gradients. In order to not map this transport error onto the resultant fluxes, a 2nd order polynomial correction is applied. Assessing the shape of this correction shows that the latitudinal gradients of the CH4_S5P_WFMD and CH4_S5P_SRONt retrievals from the commissioning phase (prior to April 2018) are somewhat

	ESA Climate Change Initiative (CCI+) Climate Assessment Report (CAR) for Climate Research Data Package 7 (CRDP#7) of the Essential Climate Variable (ECV) Greenhouse Gases (GHG)	Page 7
		Version 1.1
		20 March 2023

different than the same months in following years. After this, the shape of the bias correction is roughly stable for each month, allowing for a bias correction to be projected onto more recent satellite measurements, when surface measurements are not available as a constraint. No land-sea bias is seen in the derived bias correction for CH4_S5P_WFMD, and the two different GOSAT-2 retrievals (SRFP and SRPR) also result in similar curves. Some larger differences are seen for the CH4_S5P_SRON retrieval, particularly at higher latitudes, suggesting some problems in the retrieval, potentially related to snow cover.


Inversions were carried out using CH4_S5P_WFMD, CH4_S5P_SRON, and CH4_S5P_SRONt from January 2018 through December 2020. This period was chosen due to the limited availability of surface data beyond mid-2020 and the lower quality and gaps in the satellite retrievals during the commissioning phase.

The assimilation of the S5P retrievals in the Jena CarboScope global inversion system results in methane fluxes that are substantially different in spatial distribution from those obtained by the assimilation of surface air-sample measurements, but in general agreement with each other. The resultant global mean near-surface concentrations show comparable variability to and good correlation with global mean concentration estimates from NOAA and WDCGG, based on in-situ measurements. The time period is quite short, making it difficult to make robust conclusions about the derived global growth rates, but also here the results between the different inversions are statistically consistent with one another.


Many of the inferred flux increments appear plausible, as they are related to areas with considerable uncertainty in the surface fluxes and with a poor data coverage in the surface-based measurement network. Both the CH4_S5P_WFMD and CH4_S5P_SRON retrievals show a decrease in methane fluxes over much of China and India (compared to the prior and more pronounced than in the surface-based inversion), and an increase in emissions in the Middle East and/or Central Asia. Reduced methane emissions are inferred for both Boreal Eurasia and North America, with less agreement in the direction of the increments over the Tropics. In general, the results from the SRON retrievals were noisier than those from the WFMD product, which may be the result of the much lower reported measurement uncertainty.

In the assessment of global mean near-surface concentration, the CH4_S5P_WFMD inversion correlated slightly better with both the surface-based inversion and the NOAA and WDCGG estimates, suggesting a slightly better consistency with the surface measurements on a global scale.

The concentration fields resulting from the optimized fluxes were compared to independent measurements, namely aircraft profiles and total column measurements from the TCCON network of surface-based Fourier Transform Spectrometers. These results show that that satellite-based inversions agree better with TCCON than does the surface-based inversion, while the aircraft-based measurements tend to agree better with the concentrations constrained from the surface network.

	ESA Climate Change Initiative (CCI+)		Page 8
	Climate Assessment Report (CAR)		
	for Climate Research Data Package 7 (CRDP#7)		Version 1.1
	of the Essential Climate Variable (ECV) Greenhouse Gases (GHG)		20 March 2023

Some of the unphysical or unlikely flux results can be ameliorated by changing the settings of the inversion system: e.g. increasing temporal and spatial correlation lengths, inflating the estimated model-data mismatch error, or giving more weight to the prior. Simultaneously assimilating surface-based and satellite measurements may also help to anchor the model to a more physical result. For the scientific interpretation of the satellite retrievals, this will be required. The assessment presented here simply draws attention to the current retrievals are not (yet) fully consistent with our knowledge of the surface fluxes based on surface measurements.


	ESA Climate Change Initiative (CCI+)		Page 9
	Climate Assessment Report (CAR)		
	for Climate Research Data Package 7 (CRDP#7)		Version 1.1
	of the Essential Climate Variable (ECV) Greenhouse Gases (GHG)		20 March 2023

2. User related aspects discussed in the peer-reviewed literature

The GHG-CCI project primarily aims at bringing new knowledge about the sources and sinks of CO₂ and CH₄ based on satellite-derived data products. Since the start of Phase 1 of the GHG-CCI pre-cursor project in 2010, this aspect has been addressed in a series of publications, which are shortly summarised in the following. They usefully provide the background for the new studies that have been performed specifically for this report and that will be described next. For a full list of publications see “Project publications” on <https://climate.esa.int/en/projects/ghgs/publications/>.

We start with the publications related to natural CO₂ fluxes.

- Using global GOSAT XCO₂ retrievals, Basu et al. (2013) presented first global CO₂ surface flux inverse modelling results for various regions. Their analysis suggested a reduced global land sink and a shift of the carbon uptake from the tropics to the extra-tropics. In particular, their results suggested that Europe is a stronger carbon sink than expected, but this feature was not further discussed in this paper.
- Chevallier et al. (2014a) analysed an ensemble of global inversion results assimilating two GOSAT XCO₂ retrieval products. They found hemispheric and regional differences in posterior flux estimates that are beyond 1 sigma uncertainties. They too found a significantly larger European carbon sink or a larger North African emission than expected. They concluded to the existence of significant flaws in all main components of the inversions: the transport model, the prior error statistics and the retrievals.
- Houweling et al. (2015) presented the outcome of a large inverse modelling intercomparison experiment on the use of GOSAT retrievals. The ensemble of results confirmed the large latitudinal shift in carbon uptake, but they showed that the reduced gradient degrades the agreement with background aircraft and surface measurements.
- Reuter et al. (2014a) investigated the European carbon sink further with another ensemble of GOSAT XCO₂ products, a SCIAMACHY XCO₂ product and a new inversion method which is less sensitive to some of the issues discussed in Chevallier et al. (2014a). Reuter et al. (2014a) only used satellite XCO₂ retrievals over Europe to rule out that non-European satellite data adversely influence the European results and they also only used short-term (days) transport modelling to avoid long-range transport errors. Based on an extensive analysis they concluded: “We show that the satellite-derived European terrestrial carbon sink is indeed much larger (1.02 ± 0.30 GtC/year in 2010) than previously expected”. The value they derived is significantly larger compared to bottom-up estimates (not based on atmospheric measurements) of 0.235 ± 0.05 GtC/year for 2001-2004 (Schulze et al, 2009).
- The findings of Reuter et al. (2014a) stimulated additional research (Feng et al. 2016a, Reuter et al. 2016c).
- Detmers et al. (2015) analyzed GOSAT XCO₂ retrievals to detect and quantify anomalously large carbon uptake in Australia during a strong La Niña episode.
- For flux inversions not only the retrieved greenhouse gas values are relevant but also their error statistics, in particular the reported uncertainties. Chevallier and O’Dell (2013) analyzed this aspect in the context of CO₂ flux inversions using GOSAT XCO₂ retrievals. For CH₄, Cressot et al. (2013, 2016) studied the uncertainty of flux inversions assimilating SCIAMACHY, GOSAT or IASI XCH₄ retrievals.
- Focussing on Canadian and Siberian boreal forests, Schneising et al. (2011) computed longitudinal XCO₂ gradients from SCIAMACHY XCO₂ retrievals during the vegetation growing season over Canadian and Siberian boreal forests and compared the gradients with outputs from NOAA’s CO₂ assimilation system CarbonTracker (Peters et al. 2007). They found good agreement for the total


	ESA Climate Change Initiative (CCI+) Climate Assessment Report (CAR) for Climate Research Data Package 7 (CRDP#7) of the Essential Climate Variable (ECV) Greenhouse Gases (GHG)	Page 10
		Version 1.1
		20 March 2023

boreal region and for inter-annual variations. For the individual regions, however, they found systematic differences suggesting a stronger Canadian boreal forest growing season CO₂ uptake and a weaker Siberian forest uptake compared to CarbonTracker.

- Focussing on hemispheric data and on carbon-climate feedbacks, Schneising et al. (2014a) used SCIAMACHY XCO₂ to study aspects related to the terrestrial carbon sink by looking at co-variations of XCO₂ growth rates and seasonal cycle amplitudes with near-surface temperature. They found XCO₂ growth rate changes of 1.25 ± 0.32 ppm/year/K (approximately 2.7 ± 0.7 GtC/year/K; indicating less carbon uptake in warmer years, i.e., a positive carbon-climate feedback) for the Northern Hemisphere in good agreement with CarbonTracker.
- Reuter et al. (2013) computed CO₂ seasonal cycle amplitudes using various satellite XCO₂ data products (using GHG-CCI products but also GOSAT XCO₂ products generated in Japan at NIES (Yoshida et al. 2013, Oshchepkov et al. 2013) and the NASA ACOS product (O'Dell et al. 2012) and compared the amplitudes with TCCON and CarbonTracker. They found that the satellite products typically agree well with TCCON but they found significantly lower amplitudes for CarbonTracker suggesting that CarbonTracker underestimates the CO₂ seasonal cycle amplitude by approx. 1.5 ± 0.5 ppm (see also Buchwitz et al., 2015, for a discussion of these findings).
- Lindquist et al. (2015) compared satellite XCO₂ retrievals, surface XCO₂ retrievals and atmospheric model simulations in terms of XCO₂ seasonal cycle. They found that the satellite retrieval algorithms performed qualitatively similarly but showed notable scatter at most validation sites. None of the tested algorithm clearly outperformed another. They showed that the XCO₂ seasonal cycle depends on longitude especially at the mid-latitudes, which was only partially shown by the models. They also found that model-to-model differences could be larger than GOSAT-to-model differences.
- Guerlet et al. (2013a) analyzed GOSAT XCO₂ retrievals focusing on the Northern Hemisphere. They identified a reduced carbon uptake in the summer of 2010 and found that this is most likely due to the heat wave in Eurasia driving biospheric fluxes and fire emissions. Using a joint inversion of GOSAT and surface data, they estimated an integrated biospheric and fire emission anomaly in April–September of 0.89 ± 0.20 PgC over Eurasia. They found that inversions of surface measurements alone fail to replicate the observed XCO₂ inter-annual variability (IAV) and underestimate emission IAV over Eurasia. They highlighted the value of GOSAT XCO₂ in constraining the response of land-atmosphere exchange of CO₂ to climate events.
- Basu et al. (2014) studied seasonal variation of CO₂ fluxes during 2009–2011 over Tropical Asia using GOSAT, CONTRAIL and IASI data. They found an enhanced source for 2010 and concluded that this is likely due to biosphere response to above-average temperatures in 2010 and unlikely due to biomass burning emissions.
- Parazoo et al. (2013) used GOSAT XCO₂ and solar induced chlorophyll fluorescence (SIF) retrievals to better understand the carbon balance of southern Amazonia.
- Ross et al. (2013) used GOSAT data to obtain information on wildfire CH₄:CO₂ emission ratios.

Despite the fact that none of the existing satellite missions has been optimized to obtain information on anthropogenic CO₂ emissions, this important aspect has been addressed in several recent publications using existing satellite XCO₂ products.

- Schneising et al. (2013) presented an assessment of the satellite data over major anthropogenic CO₂ source regions. They used a multi-year SCIAMACHY XCO₂ data set and compared the regional XCO₂ enhancements and trends with the emission inventory EDGAR v4.2 (Olivier et al. 2012). They found no significant trend for the Rhine-Ruhr area in central Europe and the US East Coast but a significant


	ESA Climate Change Initiative (CCI+) Climate Assessment Report (CAR) for Climate Research Data Package 7 (CRDP#7) of the Essential Climate Variable (ECV) Greenhouse Gases (GHG)	Page 11
		Version 1.1
		20 March 2023

increasing trend for the Yangtze River Delta in China of about $13 \pm 8\%$ /year, in agreement with EDGAR ($10 \pm 1\%$ /year).

- Reuter et al. (2014b) studied co-located SCIAMACHY XCO₂ and NO₂ retrievals over major anthropogenic source regions. For East Asia they found increasing emissions of NO_x (+5.8%/year) and CO₂ (+9.8%/year), i.e., decreasing emissions of NO_x relative to CO₂ indicating that the recently installed and renewed technology in East Asia, such as power plants and transportation, is cleaner in terms of NO_x emissions than the old infrastructure, and roughly matches relative emission levels in North America and Europe.

A series of studies have also addressed methane emissions.

- SCIAMACHY data have already been extensively used to improve our knowledge on regional methane emissions prior to the start of the GHG-CCI project (e.g., Bergamaschi et al. 2009). A more recent research focus was to shed light on the unexpected renewed atmospheric methane increase during 2007 and later years using ground-based and satellite data (e.g., Rigby et al. 2008, Dlugokencky et al. 2009, Bergamaschi et al. 2009, 2013, Schneising et al. 2011, Frankenberg et al. 2011, Sussmann et al. 2012, Crevoisier et al. 2013). Based on an analysis of SCIAMACHY year 2003–2009 retrievals an increase of 7–9 ppb/year (0.4–0.5%/year) has been found with the largest increases in the tropics and northern mid latitudes (Schneising et al. 2011) but a particular region responsible for the increase has not been identified (Schneising et al. 2011; Frankenberg et al. 2011). Bergamaschi et al. (2013) used SCIAMACHY retrievals and NOAA surface data for 2003–2010 and inverse modelling in order to attribute the observed increase of atmospheric concentrations to changes in emissions. They concluded that most of this increase is due to emissions in the Tropics and the mid-latitudes of the northern hemisphere, while no significant trend was derived for Arctic latitudes. The increase is mainly attributed to anthropogenic sources, superimposed with significant inter-annual variations of emissions from wetlands and biomass burning.
- Methane emissions have also been obtained from GOSAT, as presented in a number of publications as shown in, e.g., Fraser et al. (2013, 2014), Monteil et al. (2013), Cressot et al. (2014), Alexe et al. (2015), Turner et al. (2015) and Pandey et al. (2016). Note that for these studies often CH₄ retrievals from several satellites have been used (as well as NOAA data), e.g., Monteil et al. (2013), and Alexe et al. (2015) used SCIAMACHY and GOSAT retrievals and Cressot et al. (2014, 2016) used GOSAT, SCIAMACHY and IASI. Alexe et al. (2015) showed that the different satellite products resulted in relatively consistent spatial flux adjustment patterns, particularly across equatorial Africa and North America. Over North America, the satellite inversions result in a significant redistribution of emissions from North-East to South-Central USA, most likely due to natural gas production facilities.
- Several publications focused on (relatively localized) methane sources in the United States: For example, Schneising et al. (2014b) analyzed SCIAMACHY data over major US “fracking” areas and quantified methane emissions and leakage rates. For two of the fastest growing production regions in the US, the Bakken and Eagle Ford formations, they estimated that emissions increased by 990 ± 650 ktCH₄/year and 530 ± 330 ktCH₄/year between the periods 2006–2008 and 2009–2011. Relative to the respective increases in oil and gas production, these emission estimates correspond to leakages of $10.1\% \pm 7.3\%$ and $9.1\% \pm 6.2\%$ in terms of energy content, calling immediate climate benefit into question and indicating that current inventories likely underestimate the fugitive emissions from Bakken and Eagle Ford. Others also used SCIAMACHY data over the US to identify and quantify localized anthropogenic methane emission sources (Kort et al. 2014, Wecht et al. 2014). Last, Turner et al. (2015) used GOSAT retrievals within a meso-scale inversion system for the US.

	ESA Climate Change Initiative (CCI+)		Page 12
	Climate Assessment Report (CAR) for Climate Research Data Package 7 (CRDP#7)		
			Version 1.1
	of the Essential Climate Variable (ECV) Greenhouse Gases (GHG)		20 March 2023

The SCIAMACHY XCH₄ retrievals have also been used to improve chemistry-climate models (Shindell et al. 2013, Hayman et al. 2014). For a more recent publication on localized emission sources please see Schneising et al., 2020, and additional publications as listed in the publication list provided by the GHG-CCI+ website (<https://climate.esa.int/en/projects/ghgs/publications/>).

3. Assessment of satellite-derived XCO₂ products

3.1. Introduction

Given a decade (since Basu et al., 2013, see Section 2) of global inverse modelling studies assimilating real XCO₂ retrievals, extended to 1.5 decades (Chevallier et al., 2005) in the case of partial column CO₂ retrievals, the current interest in XCO₂ products for global inverse modelling is about multi-year global products. This has not been always the case (Chevallier et al., 2011). The first four GHG-CCI Climate Research Data Packages fulfilled this ambition with SCIAMACHY and TANSO retrievals.

The 5th, 6th and 7th GHG-CCI+ Climate Research Data Packages (CRDP#5, #6 and #7, <http://cci.esa.int/ghg#data>) include three CO₂ products:


- CO2_OC2_FOCA: retrieved from OCO-2 using University of Bremen's FOCAL algorithm
- CO2_TAN_OCFP: retrieved from TanSat using University of Leicester's UoL-FP (or OCFP) algorithm
- CO2_GO2_SRFP: retrieved from GOSAT-2 using SRON's RemoTeC (or SRFP) algorithm

Their latest versions are evaluated in this chapter within a forward and inverse modelling framework. For the inverse framework, comparisons are made with the surface air-sample-driven inversion and the satellite-driven inversion of the Copernicus Atmosphere Monitoring Service (<https://atmosphere.copernicus.eu/>, Chevallier et al., 2021a, 2021b). The latter assimilated version 10 of the official bias-corrected XCO₂ retrievals made by the NASA Atmospheric CO₂ Observations from Space (ACOS) algorithm described by Osterman et al. (2020).

The evaluated product from CRDP#7 is summarized in Table 1 below. The three official bias-corrected products have been processed by LSCE on the supercomputer Irene of <http://www-hpc.cea.fr/en/complexe/tgcc.htm>. In addition to test runs, two inversions have been performed twice: the OCFP-driven inversion was done initially with v1.1 and the FOCAL-driven inversion was performed in a configuration that excluded ocean retrievals. Only the best results are presented here (OCFP v1.2 and FOCAL with ocean retrievals, respectively).

Product ID	Satellite	Algorithm	Data provider	Reference	Period available	Evaluators (sections)
CO2_OC2_FOCA	OCO-2	FOCAL, v10	IUP, Univ. Bremen	Reuter et al., 2017a, 2017b	09/2014-03/2021	LSCE (3.2, 3.3)
CO2_TAN_OCFP	TanSat	OCFP, v1.2	Univ. of Leicester	Yang et al., 2021	03/2017-04/2018	LSCE (3.2, 3.3)
CO2_GO2_SRFP	GOSAT-2	SRFP, v2.0.0	SRON	Krisna et al., 2022a	02/2019-08/2020	LSCE (3.2, 3.3)

Table 1. XCO₂ products evaluated in this report.

	ESA Climate Change Initiative (CCI+) Climate Assessment Report (CAR) for Climate Research Data Package 7 (CRDP#7) of the Essential Climate Variable (ECV) Greenhouse Gases (GHG)	Page 14
		Version 1.1
		20 March 2023

3.2. Comparisons with forward model simulations

3.2.1. Method

In this section, we compare CO₂_OC2_FOCA, CO₂_TAN_OCFP and CO₂_GO2_SRFP with a forward simulation of the LMDz transport model (Hourdin et al. 2013) nudged to the ERA5 reanalysis and using surface fluxes from a classical atmospheric inversion that assimilated surface air-sample measurements. Our forward simulation comes from the CAMS CO₂ inversion product driven by surface air-sample measurements (version 20r2, <https://atmosphere.copernicus.eu/>), an earlier version of which was described by Chevallier et al. (2010a). It uses the LMDz transport model with a recent configuration of the model physics (Remaud et al., 2018). In space, the model is discretized into 39 vertical layers, 3.75 longitude degrees and 1.9 latitude degrees. Compared to ground retrievals from the Total Carbon Column Observing Network (TCCON, Wunch et al., 2011) for the 2004-2020 period, absolute biases are less than 1 ppm at most sites (exceptions are Manaus, Izana, Hefei, Saga, JPL, Pasadena, Four Corners, Park Falls, Paris, Eureka), and the standard deviation is usually about 1 ppm, exceptionally reaching 2.2 ppm at the Zugspitze mountain site (Chevallier, 2021a). The standard deviation of the model-minus-TCCON differences, resulting from both model and retrieval errors, is therefore smaller than the satellite retrieval Bayesian uncertainty in the CRDP#7 products (e.g., for FOCAL, $1\sigma \sim 1.7$ ppm) but also larger than the reported ACOS Bayesian uncertainty ($1\sigma \sim 0.5$ ppm).

When comparing XCO₂ model and satellite retrievals, we account for the prior profiles and the averaging kernels of each individual retrieval. The satellite retrievals have much higher spatial resolution than the global LMDz model, by several orders of magnitude (the ground resolution of, e.g., OCO-2 soundings is around 3 km²), but in this section, we use them individually, without any averaging, in contrast to the next section about inverse modelling. For both each retrieval product, we compute the statistics of their difference with the model simulation in three latitude bands: the latitudes north of 25°N, the latitudes south of 25°S and the latitudes between 25°S and 25°N. We also stratify the results per geotype (land and water). All statistics relate to the full period covered by each CRDP#7 product, except for FOCAL which ends 3 months after the end of the benchmark CAMS inversion v20r2 (March 2021 vs. December 2020): the last 3 months have therefore not been used in this section. The inversion section does not share this temporal limitation.

3.2.2. Results

The results are summarized in Figure 1. Since we have no way to distinguish between random errors and systematic ones in the retrieval products and in the forward simulation, and following the usual practice (e.g., Desroziers et al. 2005), we use the root mean square (RMS) to characterize the statistics of the model-minus-observation departures, rather than the standard deviation.

**Climate Assessment Report (CAR)**
for Climate Research Data Package 7 (CRDP#7)

Version 1.1

of the Essential Climate Variable (ECV)
Greenhouse Gases (GHG)

20 March 2023

The number of data feeding the statistics (the pink bars in Figure 1) varies with the instrument, the screening performed in the corresponding retrieval algorithm and the length of the period. The RMS departures (the purple disks in Figure 1) are quite different among the three products, but each product shows values larger than 2 ppm in at least two zonal-band/geotype categories each time. Values around 1 ppm are seen only over the ocean for CO₂_OC2_FOCA. An RMS value larger than 3 ppm is seen for CO₂_GO2_SRFP in the northern extra-Tropical band. These values seem to confirm the greater uncertainty of the CRDP#7 products compared to ACOS product (with RMS values of 0.6 – 1.3 ppm, Chevallier and Marshall, 2021, their Figure 1), that was suggested by the difference in reported Bayesian uncertainty (see Section 3.2.1).

The precision and bias of the CRDP#7 products have been assessed independently in the Product Validation and Intercomparison Report (PVIR, Table 1-1, Buchwitz et al. 2022) based on TCCON observations. We note that the scatter of the retrieval misfits to TCCON presented in the PVIR is smaller than the scatter of the retrieval RMS differences to the model presented here by about 25%, without any obvious explanation yet: the use of the scaled median absolute deviation rather than the standard deviation in the PVIR may play a role; also, the statistics here cover a much larger area than the vicinity of the TCCON stations.

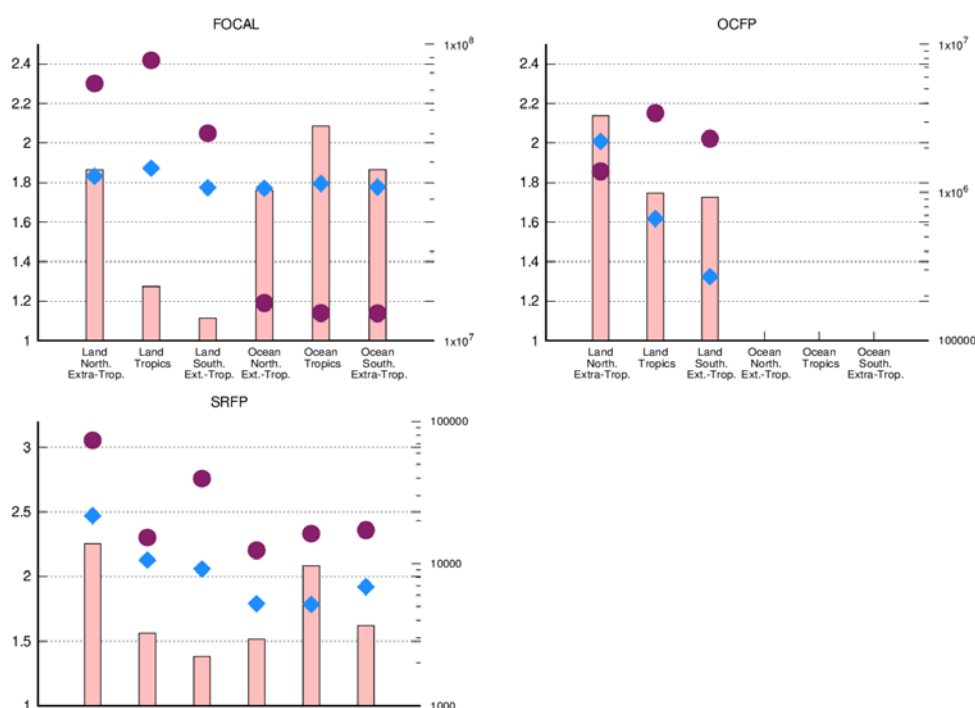



Figure 1. The purple disks show the Root Mean Squared values (RMS) of the misfits between the three XCO₂ products indicated in the plot titles and the reference CAMS surface-driven simulation for the period covered by each product (minus the 3 months of 2021 for FOCAL, as indicated in the text). The blue squares represent the root mean square of the sum of the CAMS simulation error variances and of the retrieval error variances. The globe is divided into three latitude bands. Land and ocean data are also separated. The number of data included in the statistics is reported as vertical pink bars with a logscale axis on the right.

	ESA Climate Change Initiative (CCI+) Climate Assessment Report (CAR) for Climate Research Data Package 7 (CRDP#7) of the Essential Climate Variable (ECV) Greenhouse Gases (GHG)	Page 16
		Version 1.1
		20 March 2023

We now compare the RMS values of Figure 1 with the “bottom-up” quadratic sum of their components (the blue squares in Figure 1): the retrieval Bayesian uncertainty and the model uncertainty. We refer to Chevallier and O’Dell (2013) for more background about the underlying principles. We take the retrieval Bayesian uncertainty directly from the product data files. Following the approach described in Chevallier and O’Dell (2003), we estimate the 1σ model uncertainty to be about 0.6 ppm, a value which is consistent with the model-minus-TCCON differences seen at most non-urban sites, given TCCON retrieval uncertainty (Chevallier, 2021a).

Figure 1 suggests that the bottom-up error budget is underestimated for all three products, except for the ocean retrievals of CO2_OC2_FOCA, that show better values than reported. The overall underestimation likely reflects underestimated retrieval precision, because the retrieval uncertainty already dominates the error budget. The underestimation of the reported retrieval uncertainty in all three products (at least over land) is a different conclusion than the PVIR one on this topic.


3.3. Inversion experiments with the LSCE system

3.3.1. Method

In this section, we go one step further in the evaluation of the CRDP#7 products with the LSCE system by interpreting the model-data misfits shown in Section 3.2 in terms of surface fluxes. The satellite data are assimilated alone, without combining them with other observations, in order to focus on their own signals. In order to avoid numerical artifacts caused by the much higher spatial resolution of the CO2_OC2_FOCA and CO2_TAN_OCFP retrievals than the LMDz model, we follow Crowell et al. (2019) by aggregating these retrievals in 10-second intervals, that roughly correspond to boxes of $67 \times 10 \text{ km}^2$ for OCO-2, a surface area which is still much smaller than the individual model grid boxes of $3.75^\circ \times 1.9^\circ$. This approach was also used in the CAMS OCO-2-driven inversion FT20r3 used here.

We use the three CRDP#7 products candidly, i.e. without modifying the retrieval values and their associated uncertainty in input to the 10-s binning algorithm. However, if several 10-s-binned retrievals of a same orbit fall within the same model grid box, we inflate the variance of the retrieval errors by the number of concerned 10-s-binned retrievals, in order to avoid likely local error correlations (at least from the transport model). As in the previous section, we use the retrieval averaging kernels and prior profiles when assimilating them. As an example, processing the full multi-year series of CO2_OC2_FOCA within the inverse system required about 10 days of computation on 70 parallel CPU cores on the supercomputer of TGCC.

The fluxes inferred from CO2_OC2_FOCA, CO2_TAN_OCFP and CO2_GO2_SRFP are compared to two benchmark inversion: the CAMS official inversion products v20r2 (used in Section 3.2) that exclusively assimilated 159 sites of surface air-sample measurements from the Global Atmosphere Watch programme, and the CAMS official inversion product FT20r3 that exclusively assimilated the ACOS OCO-2 retrievals over land. Ocean glint retrievals were not assimilated in FT20r3 because of likely systematic errors (Chevallier et al., 2019), but such a selection is not done for the CRDP#7

	ESA Climate Change Initiative (CCI+)		Page 17
	Climate Assessment Report (CAR) for Climate Research Data Package 7 (CRDP#7)		
			Version 1.1
	of the Essential Climate Variable (ECV) Greenhouse Gases (GHG)		20 March 2023

products here in the absence of similar evidence. Actually, we made a test without the ocean data of CO2_OC2_FOCA, but results were found less realistic than with these (see Section 3.3.2).

The inversion system works at the grid-point weekly scale and generates a large volume of data. The present comparison focuses on a few key quantities: (i) the global annual growth rate that is well known from the NOAA marine surface data (Conway et al. 1994, <http://www.esrl.noaa.gov/gmd/ccgg/trends/global.html>), (ii) the grid-point annual-total fluxes, (iii) zonal annual CO₂ budgets.

3.3.2. Global annual atmospheric growth rates

In 2019, the Inverse modelling protocol for the annual global carbon budget of the Global Carbon Project (GCP) started to use a quality criterion on the global annual atmospheric growth rate of the inversion (Chevallier et al. 2019, 2020, 2021): “using a conversion factor, the series of annual fluxes will be compared to the annual trend of globally-averaged marine measurements (<http://www.esrl.noaa.gov/gmd/ccgg/trends/>). Submissions that show notably different interannual variations will be excluded.”

The OCO-2 Science team's Model Intercomparison Project v10 (MIPv10) is adopting a criterion on the mean growth rate for the inversion products it gathers for the Global Stocktake: it requires the selected inversions to have a growth rate over 2015-2020 equal to 2.54 ± 0.08 ppm/a, based on NOAA's reference estimate (Brendan Byrne, personal communication, 4 January 2022). This criterion is quantitative, in contrast to the GCP one, but it is limited to the mean value: it just checks that the model simulation does not diverge over time.


In all previous CARs, poor inversion results were associated to poor inversion annual growth rates in terms of bias and/or standard deviation.

Over the six years 2015-2020, the CAMS satellite inversion FT20r3 fits NOAA's numbers (as of 16 February 2022) with a bias of -0.06 ppm/a and a standard deviation of 0.11 ppm/a¹. Its surface-driven counterpart (v20r2) shows similar statistics: -0.02 ± 0.14 ppm/a². The FOCAL-driven inversion is at 0.03 ± 0.23 ppm/a (0.06 ± 0.30 ppm/a when we exclude the ocean retrievals from the inversion, as is actually done in FT20r3). This represents a small improvement compared to the version of the previous CRDP (-0.03 ± 0.27 ppm for 2015-2019 in CRDP#6 vs. $+0.04 \pm 0.25$ ppm here for the same period). With or without the ocean retrievals, the FOCAL inversion passes the MIPv10 mean-growth-rate criterion.

For the OCFP-driven inversion, we focus on the period April 2017 – March 2018, leaving 1 month of retrievals for spin-up and 1 month for spin-down. NOAA's value for the growth rate is of 2.46 ppm/a,

¹ We assume a conversion factor of 2.086 GtC·ppm⁻¹, from Prather (2012), which may be slightly different from other studies.

² Note that the NOAA estimate and the surface-driven CAMS one are not independent since the surface-driven CAMS inversion assimilates the individual NOAA measurements

	ESA Climate Change Initiative (CCI+) Climate Assessment Report (CAR) for Climate Research Data Package 7 (CRDP#7) of the Essential Climate Variable (ECV) Greenhouse Gases (GHG)	Page 18
		Version 1.1
		20 March 2023

the OCFP-driven inversion says 2.30 ppm/a, the CAMS satellite inversion FT20r3 says 2.29 ppm/a and the CAMS air-sample inversion says 2.35 ppm/a.

For the SRFP-driven inversion, we consider the 12 months from June 2019 until May 2020, which leaves 4 months of retrievals for spin-up and 3 months for spin-down. NOAA's value for the growth rate is of 2.41 ppm/a, the SRFP-driven inversion says 1.64 ppm/a only. The CAMS satellite inversion FT20r3 and air-sample inversion v20r2 surround the NOAA value with 2.29 ppm/a and 2.59 ppm/a, respectively.

From these results, we note that only the OCFP inversion approaches the NOAA growth rate as well as the CAMS inversions. The SRFP inversion has a much smaller value and the FOCAL inversion shows a much larger standard deviation of the differences, which could be linked to the large RMS differences to the CAMS reference simulation noted in Section 3.2.2.

3.3.3. Maps of annual budgets

Figure 2 and Figure 3 display the maps of the inferred annual budgets of natural CO₂ fluxes for two 12-month periods that overlap with either CO₂_TAN_OCFP or CO₂_GO2_SRFP. CO₂_OCO_FOCA is available on both. The figures also display the maps for the two CAMS inversions. As shown already by Chevallier et al. (2019), the two CAMS inversions have rather comparable flux patterns in the northern extra-Tropics, but the ACOS-driven inversion has more spatial gradients than the surface-driven one in the Tropical lands where the surface measurement network is particularly sparse. The three CRDP#7-driven inversions have even larger gradients there (Australia excepted), but also in the northern extra-Tropics. The colour bar has actually not been adapted to their variability. Surprisingly, the spatial patterns (irrespective of their amplitude) are similar between the four satellite-driven inversions over land. Over the ocean, the two CAMS inversions are close to each other, but changes in the spread of Tropical ocean outgassing regions are seen with the assimilation of CO₂_TAN_OCFP and CO₂_OC2_FOCA. CO₂_TAN_OCFP widely extends the outgassing regions while CO₂_OC2_FOCA dramatically reduces them in the Atlantic.

Climate Assessment Report (CAR) for Climate Research Data Package 7 (CRDP#7)

Version 1.1

of the Essential Climate Variable (ECV)
Greenhouse Gases (GHG)

20 March 2023

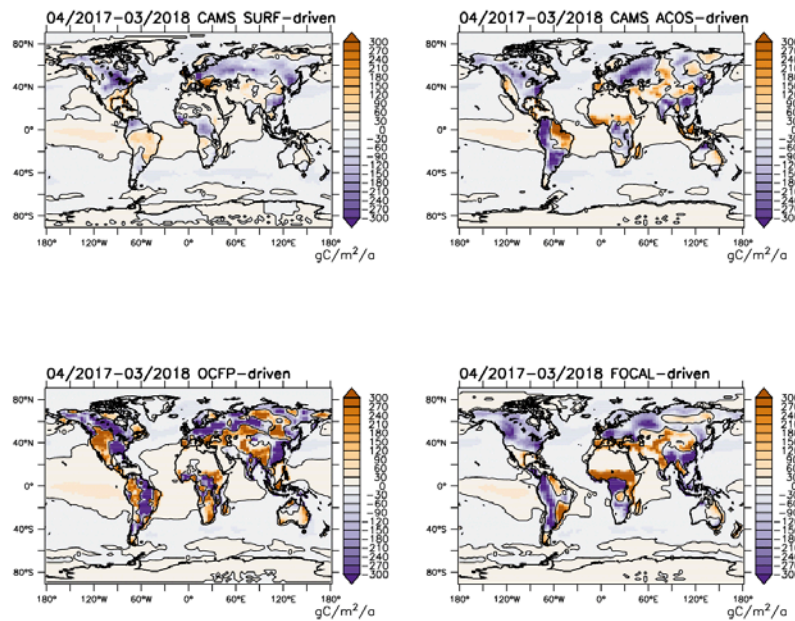


Figure 2. Grid-point budget of the natural CO₂ fluxes for the period April 2017 – March 2018, for the two CAMS inversions for the FOCAL inversion and for the OCFP inversion. In the sign convention, positive fluxes correspond to a net carbon source into the atmosphere.

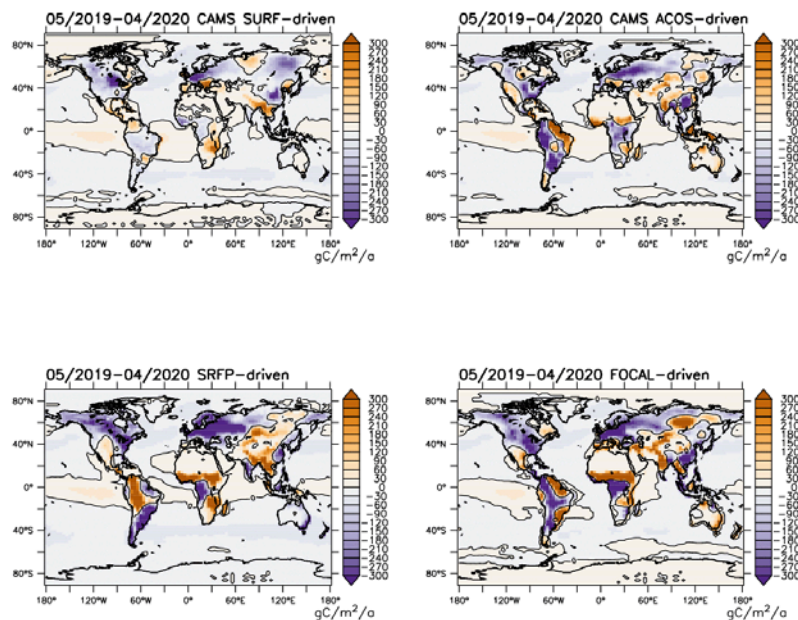



Figure 3. Grid-point budget of the natural CO₂ fluxes for the period May 2019 – April 2020, for the two CAMS inversions for the FOCAL inversion and for the SRFP inversion. In the sign convention, positive fluxes correspond to a net carbon source into the atmosphere.

	ESA Climate Change Initiative (CCI+) Climate Assessment Report (CAR) for Climate Research Data Package 7 (CRDP#7) of the Essential Climate Variable (ECV) Greenhouse Gases (GHG)	Page 20
		Version 1.1
		20 March 2023

3.3.4. Annual budget time series

The time series of the annual natural carbon budgets at several very broad scales are displayed in Figure 4 for the period between 2015 and 2020: the globe, the northern or southern extra-Tropics, and the Tropics with lands and oceans either separated or combined. At the global scale (top row), the curves reflect the growth rate discussed in Section 3.3.2, but without the fossil fuel and cement flux component: recognize the larger variability of CO2_OC2_FOCA, the small growth rate of CO2_GO2_SRFP and the “good” one of CO2_TAN_OCFP. The CAMS ACOS inversion remains close to the CAMS surface inversion in all subplots, which is less the case for the three CRDP#7 inversions.

The five inversions locate the land sink mostly in the northern extra-Tropics (middle row), even though a large year-to-year variability is seen in the Tropics. The southern extra-Tropical lands (that represent a relatively small surface area) are close to neutral each year. We notice the very large latitudinal gradient over land obtained with CO2_GO2_SRFP: a strong sink in the extra-Tropics and a strong source in the Tropics. CO2_TAN_OCFP yields a gradient which is consistent with the CAMS inversions. This is slightly less the case with CO2_OC2_FOCA after 2017 when the red curve diverges from the blue and orange ones in the Tropical and the extra-Tropical lands.

The global ocean sink inferred from CO2_GO2_SRFP and CO2_TAN_OCFP is very different from the CAMS inversions and from the CO2_OC2_FOCA inversion. It is actually either too large (SRFP) or too weak (OCFP) to be defensible from a biogeochemical point of view (Friedlingstein et al., 2021). For CO2_OC2_FOCA, we notice latitudinal differences to CAMS, with less source in the Tropics (as noted about Figure 2 and Figure 3) and less sink in the Southern extra-Tropics.

Climate Assessment Report (CAR) for Climate Research Data Package 7 (CRDP#7)

of the Essential Climate Variable (ECV)
Greenhouse Gases (GHG)

Version 1.1

20 March 2023

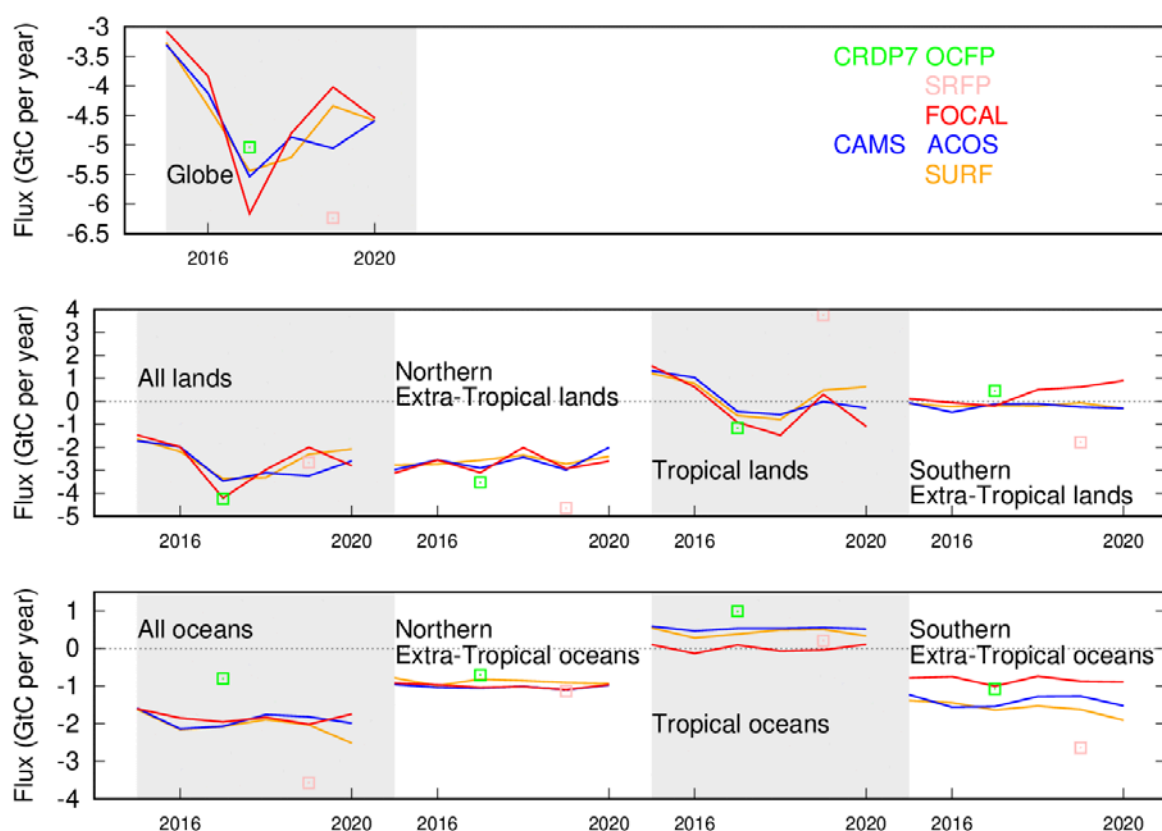



Figure 4. Inferred natural CO₂ annual flux (without fossil fuel emissions) averaged over the globe or over all lands or oceans. In the case of lands and oceans, three broad latitude bands are also defined: northern extra-Tropics (north of 25°N), Tropics (within 25° of the Equator), and southern extra-Tropics (south of 25°S). The blue and orange curves correspond to the CAMS surface-driven (SURF) and OCO-2-driven (ACOS) products. In the sign convention, positive fluxes correspond to a net carbon source into the atmosphere.

3.3.5. Conclusions

The assimilation of the CRDP#7 products in the LSCE global inversion system infers CO₂ surface fluxes that are very different from those obtained by both the assimilation of surface air-sample measurements and the assimilation of NASA's retrievals from OCO-2. We think that they are less credible on the basis of current knowledge of the carbon cycle (e.g., Friedlingstein et al 2021). We particularly highlighted the atmospheric growth rate and the ocean outgassing regions (see, e.g., the Global ocean surface carbon product of the Copernicus Marine Environment Monitoring Service³). We also related these features to the relatively large differences of the CRDP#7 products to the CAMS reference surface air-sample inversion, in particular for CO₂_GO2_SRFP. The consistent results obtained in the inversion between the surface air-sample measurements and the ACOS retrievals demonstrates that there is no fundamental limitation in atmospheric inverse modelling (e.g., in the

³ <https://doi.org/10.48670/moi-00047>

	ESA Climate Change Initiative (CCI+)	Page 22
	Climate Assessment Report (CAR) for Climate Research Data Package 7 (CRDP#7)	Version 1.1
	of the Essential Climate Variable (ECV) Greenhouse Gases (GHG)	20 March 2023

realism of the transport model or in the modelled error statistics) when assimilating satellite XCO₂ retrievals. The ACOS-driven CO₂ surface fluxes have actually been part of the official CAMS data portfolio since year 2019.

ACOS and CO2_OC2_FOCA exploit the same OCO-2 spectra. The various tests performed do not allow us to identify the distinctive asset of ACOS in our system, but the dramatic increase in the CO2_OC2_FOCA data volume since CRDP#6 now excludes the data density. The following hypotheses remain: the data precision (that seem to be better for ACOS, see Section 3.2.2), the data trueness (linked to the quality of the physical retrieval scheme and to its empirical bias-correction), the accuracy of the averaging kernels (see Chevallier, 2015, for a discussion on potential issues with the averaging kernel profiles), or a combination of these qualities at once. These hypotheses implicitly involve the retrieval quality control. Detailed sensitivity tests could be performed for this, but note that our single CO2_OC2_FOCA-driven inversion already represented a large computational effort that lasted ten days on a supercomputer.


About computational effort, CO2_OC2_FOCA's distinct advantage compared to ACOS is its representation of multiple scattering effects in the radiative transfer in a form that is not costlier than absorption. In preparation for the Copernicus CO₂ Monitoring Mission that will provide even larger amount of data than OCO-2 (Pinty et al., 2017), CO2_OC2_FOCA represents an important achievement. To a smaller extent (in terms of data volume), the same can be said of CO2_TAN_OCFP. In this context and resources permitting, it would be important to document their performance in more detail in order to help prioritize future developments.

4. Assessment of satellite-derived XCH₄ data products

4.1. Introduction

The use of methane in inversions using satellite data has been well established, going back to the first retrievals using the SCIAMACHY sensor on Envisat from 2003. This has been extended with over a decade of measurements from the Japanese satellite GOSAT, offering improved stability and measurement precision, but sparser data coverage.

Global methane inversions based on satellite measurements are already long established, going back to the initial SCIAMACHY XCH₄ dataset from 2003, followed by over a decade of soundings from GOSAT, with improved stability and measurement precision, but sparser data coverage. With the launch of Sentinel-5 Precursor (S5P) in October 2017, these measurements moved from experimental measurements to an operational product, with vastly increased data density through a small footprint (7-km at nadir) and a continuous wide swath (2600 km). A year later, in October 2018, the Japanese satellite GOSAT-2 was launched, the successor to the successful GOSAT mission.

	ESA Climate Change Initiative (CCI+)	Page 23
	Climate Assessment Report (CAR) for Climate Research Data Package 7 (CRDP#7)	Version 1.1
	of the Essential Climate Variable (ECV) Greenhouse Gases (GHG)	20 March 2023

The 7th GHG-CCI+ Climate Research Data Package (CRDP#7, <https://climate.esa.int/en/projects/ghgs/#data>) includes the following three CH₄ products, resulting from these two sensors:


- CH₄_S5P_WFMD: retrieved from TROPOMI on S5P using the University of Bremen's WFMD algorithm
- CH₄_GO2_SRFp: retrieved from GOSAT-2 using SRON's full physics RemoTeC algorithm
- CH₄_GO2_SRPR: from GOSAT-2 using SRON's proxy RemoTeC algorithm, retrieving the ratio of CH₄ to CO₂

Product ID	Instrument	Algorithm	Data provider	Reference	Period available	Evaluators (sections)
CH ₄ _S5P_WFMD	TROPOMI	WFMD, v1.5	IUP, Univ. Bremen	Schneising et al., 2019	11/2017-12/2020	DLR (4.2, 1)
CH ₄ _GO2_SRFp	GOSAT-2	V2.0	SRON	Krisna et al., 2022a	02/2019-08/2020	DLR (4.2)
CH ₄ _GO2_SRPR	GOSAT-2	V2.0	SRON	Krisna et al., 2022b	02/2019-07/2020	DLR (4.2)
CH ₄ _S5P_SRON	TROPOMI	RemoTeC 2.5.0	SRON	Hu et al., 2016	04/2018-into 2022	DLR (4.2, 4.3)
CH ₄ _S5P_SRONt	TROPOMI	RemoTeC v0017	SRON	Lorente et al., 2021	11/2017-09/2021	DLR (4.2, 4.3)

Table 2: XCH₄ products evaluated in this report. Only the first three are officially members of CRDP#7, but the two SRON retrievals of S5P measurements are included for context and completeness.

The GOSAT-2 retrievals are only available from February through late summer 2020 at this point, making their use in global inversions somewhat challenging. Nonetheless, having more than a full year of measurements allows for an extended analysis of the behaviour of the data over the full year. The updated v1.5 version of the CH₄_S5P_WFMD data product is available over a longer time, from November 2017 through the end of 2020.

To enrich the comparison, the operational retrieval of XCH₄ from S5P (Hu et al., 2016) is also included in the analysis, and will be referred to as CH₄_S5P_SRON in the text, and as "SRON-oper" in figures. Additionally, the "scientific" or pre-operational SRON retrieval, based on Lorente et al. (2021), is included. This product includes some corrections for retrievals over high and low albedo scenes and updated spectroscopy, and extends the coverage into the commissioning phase. It is referred to as CH₄_S5P_SRONt (or simply SRON-v0017) in this report. The evaluated XCH₄ products are summarized in Table 2.

	ESA Climate Change Initiative (CCI+) Climate Assessment Report (CAR) for Climate Research Data Package 7 (CRDP#7) of the Essential Climate Variable (ECV) Greenhouse Gases (GHG)	Page 24
		Version 1.1
		20 March 2023

4.2. Comparisons with forward model simulations

4.2.1. Method


In this section we begin by plotting the data products themselves, to get a view of the temporal and spatial distribution. We then compare the different satellite products with concentration fields resulting from a forward simulation of the TM3 transport model (Heimann and Körner, 2003) using optimized fluxes from an inversion assimilating flask measurements from 31 surface sites. The inversion was carried out using the Jena CarboScope variational inversion system (based on Rödenbeck et al., 2003). The transport is carried out at 3.8° latitude by 5° longitude resolution and with 19 vertical levels, and is driven by meteorological fields from the ERA5 reanalysis.

Because the model transport is imperfect, especially with respect to the tropopause height and the gradient of methane within the stratosphere, the comparison to the surface-optimized fields is used to derive a model-specific bias correction. The bias correction is modelled as a 2nd order polynomial as a function of latitude and month, following the approach of Bergamaschi et al. (2007) (see Equation 4 from this paper). Because this correction is independent of longitude, the information about local gradients is largely maintained, while ensuring that the model can simultaneously interpret total-column and surface-based measurements of CH₄ in a consistent manner.

When comparing the modelled XCH₄ columns to the XCH₄ measurements, both the prior profile and the averaging kernel are taken into account. Because the spatial resolution of the S5P measurements is so much higher than that of the model fields, we average them to create super-observations for use in the inversion. This is done in the following manner:

- Count all retrievals with quality flag “good” (or, for CH₄_S5P_SRON and CH₄_S5P_SRONT, those with qa filter > 0.5) that fall within a model doxel (gridbox per orbit)
- Average the XCH₄ values, weighted by the inverse of measurement precision
- Calculate the mean averaging kernel, averaging per retrieval layer, weighted by the inverse of the measurement precision
- Determine the super-obs measurement precision, as the maximum of:
 - Double the weighted mean precision or
 - The standard deviation of the XCH₄ measurements in the doxel

Choosing the maximum between the doubled weighted mean reported precision from the retrieval product and the standard deviation of the soundings within the doxel helps balance the very different reported precision of the TROPOMI retrievals from WFMD vs. the two SRON products.

	ESA Climate Change Initiative (CCI+)	Page 25
	Climate Assessment Report (CAR) for Climate Research Data Package 7 (CRDP#7) of the Essential Climate Variable (ECV) Greenhouse Gases (GHG)	Version 1.1
		20 March 2023

4.2.2. Results

4.2.2.1. Overview of measurement coverage

The spatial and temporal coverage of the satellite retrievals considered in this section are depicted in Figure 5: TROPOMI XCH₄ retrieval products considered here (from January 2018), averaged over 1° latitude and 3-day bins. The standard deviation of the measurements within each bin is shown on the right. Both quantities are in parts per billion (ppb), or 10⁻⁹ moles CH₄/mole of dry air. From the top are shown: CH₄_S5P_WFMD, CH₄_S5P_SRON (SRON-oper), and CH₄_S5P_SRONt (SRON-v017)., from January 2018 through December 2020. The period before January 2018 is not included in this figure due gappy coverage, and the fact that they were not included in the following inversions for technical reasons (as explained in section 4.3). At first glance the TROPOMI retrievals appear quite similar, at least the structures that are captured are the same. CH₄_S5P_WFMD clearly has the best data coverage of the three, although there is a marked improvement from the SRON-oper to SRON-v017. This is partially related to the stricter data screening over land in SRON retrievals, but is dominated by the fact that the CH₄_S5P_WFMD product also performs retrievals over the ocean, greatly increasing the number of measurements. (The CH₄_S5P_SRON retrieval has no retrievals over water, and CH₄_S5P_SRONt has very few.) This also explains the larger data gap seen over the Southern Ocean in the CH₄_S5P_SRON and CH₄_S5P_SRONt products. Another difference in temporal coverage is found in early 2020: both the CH₄_S5P_SRON and CH₄_S5P_SRONt products have a gap in mid-January, 2020, with no retrievals passing the suggested quality filters from January 11th through January 18th. No such gap is found in the CH₄_S5P_WFMD retrieval product, and the number of successful retrievals per day during this period is consistent with that earlier and later in the month. This is related to the availability of the VIIRS cloud cover data that was part of the SRON-oper retrieval, and which experienced some coverage gaps in 2020. These gaps become quite dramatic towards the end of 2020, which has led to the retrieval team adapting their cloud-screening algorithm to function even in the absence of VIIRS data. This improvement can be seen in the more consistent SRON-v017 coverage through the end of 2020.

Looking to the plots on the right-hand side, it is interesting to see that the variability within a latitude band has a somewhat different structure in the the different TROPOMI retrieval products. CH₄_S5P_WFMD shows substantial variability between 30°-50° latitude throughout the year, with the most variability in the winter. This latitude band is characterized by substantial anthropogenic emissions, which explains this feature.

One feature that emerges from both the mean XCH₄ plot and the standard deviation plot for CH₄_S5P_SRON is a positive anomaly along the northernmost edge of the measurement range in late winter and spring. If true, this would be a tantalizing signal: high methane during a period when the ground is still largely frozen, and northern wetlands are assumed to be inactive (or at least less active). However, this is also a period characterized by snow and ice cover, which results in low albedo in the near infrared. This signal is not present in the CH₄_S5P_WFMD, and appears somewhat

Climate Assessment Report (CAR) for Climate Research Data Package 7 (CRDP#7)

of the Essential Climate Variable (ECV)
Greenhouse Gases (GHG)

Version 1.1

20 March 2023

weaker in the CH₄_S5P_SRONT plot, abruptly ceding to lower XCH₄ values for measurements made north of about 70° latitude. These areas also have comparatively high standard deviation within the bins.

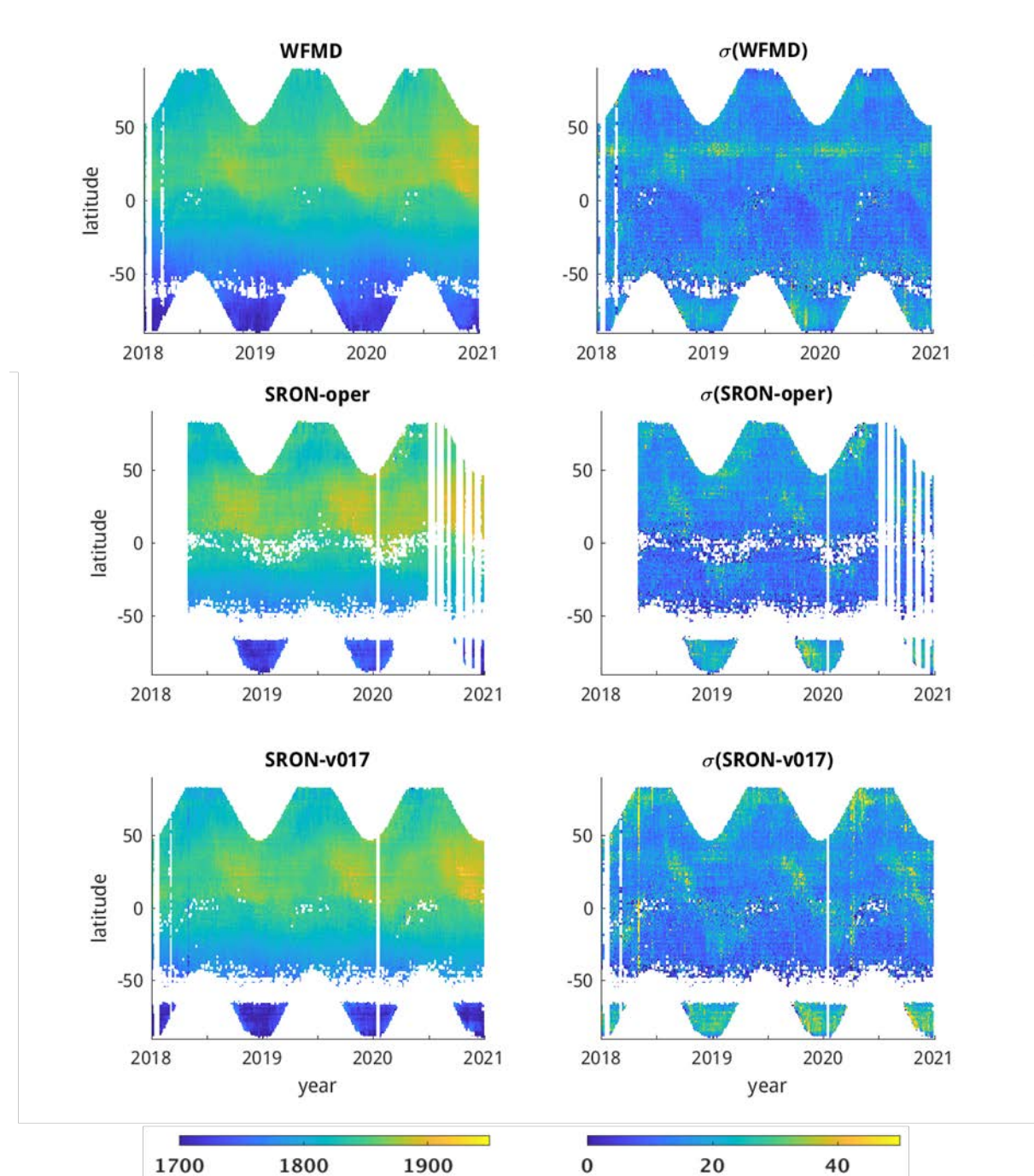


Figure 5: TROPOMI XCH₄ retrieval products considered here (from January 2018), averaged over 1° latitude and 3-day bins. The standard deviation of the measurements within each bin is shown on the right. Both quantities are in parts per billion (ppb), or 10⁻⁹ moles CH₄/mole of dry air. From the top are shown: CH₄_S5P_WFMD, CH₄_S5P_SRON (SRON-oper), and CH₄_S5P_SRONT (SRON-v017).

Similar plots showing the GOSAT-2 data coverage for the proxy and full-physics retrievals (CH₄_GO2_SRPR and CH₄_GO2_SRFP, respectively) are shown in Figure 6. As expected, the proxy product (CH₄_GO2_SRPR) has more measurements and thus, more coverage, than the full-physics retrieval (CH₄_GO2_SRFP). The proxy retrieval also exhibits higher standard deviation within the averaging bins, which might be the result of having more retrievals over areas close to emission sources of both aerosols and methane, leading to higher variability in the total column data.

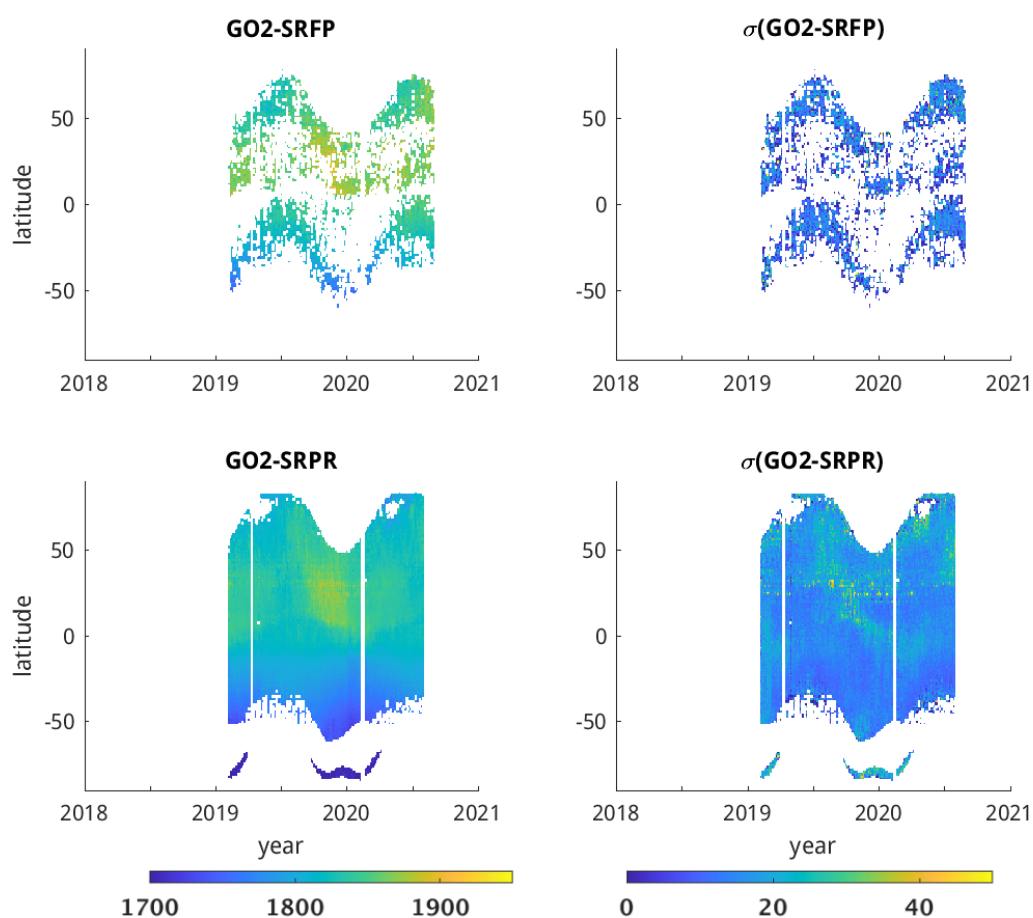


Figure 6: As Figure 5, but for the available GOSAT-2 retrievals for both the full physics retrieval (SRFP, top row) and the proxy retrieval (SRPR, lower panels).

For completeness, Figure 7 show the temporal coverage of the surface-based measurements that are used for the surface-based inversions (and for the bias correction, as described in Section 4.2.2.2 below), as well as the TCCON station data that are used for the model evaluation.



Climate Assessment Report (CAR) for Climate Research Data Package 7 (CRDP#7)

Version 1.1

of the Essential Climate Variable (ECV)
Greenhouse Gases (GHG)

20 March 2023



Figure 7: Temporal coverage of surface-based stations (left) and TCCON data (right) used for inversions and model evaluation, respectively.

4.2.2.2. Bias-correction based on surface-optimized fields

As introduced in Section 4.2.1, a 2nd-degree polynomial was fit to describe the mismatch between the XCH₄ retrievals and optimized model fields based on surface-only measurements.

In general, we expect the bias correction to have a similar shape for all the products, assuming that they are roughly consistent with each other and have similar averaging kernels, as it is accounting for errors in the model's vertical structure and/or interhemispheric gradient. Likewise, the assumption that the error can be fit by month and latitude suggests that it should be similar for the same month in subsequent years. This was not the case for the first three months of 2018, during the commissioning phase of S5P, which was shown in Fig. 16 of the previous CAR (Chevallier and Marshall, 2021). This was true for both the CH₄_S5P_SRONT and CH₄_S5P_WFMD retrievals, and implies that the data for these months should be interpreted with some caution.

The same curve-fitting was carried out for the offset between the GOSAT-2 retrievals and the surface-optimized concentration fields. The resulting bias correction curves for the SRPR and SRFP retrievals agree quite well (similar to the results in Figure 17 of CARv6).

Because the surface data were not available through to the end 2020 (as seen in Figure 7), the bias correction for the July-December 2020 was derived using the mean difference for July-December 2018 and 2019. This approach allows us to use the satellite data, which are available well before the surface measurements are, while still correcting for the model errors over this period. The resulting bias correction curves for CH₄_S5P_SRONT and CH₄_S5P_WFMD, which show no obvious discontinuity over the period in question, are shown in Figure 8.

Climate Assessment Report (CAR) for Climate Research Data Package 7 (CRDP#7)

Version 1.1

of the Essential Climate Variable (ECV)
Greenhouse Gases (GHG)

20 March 2023

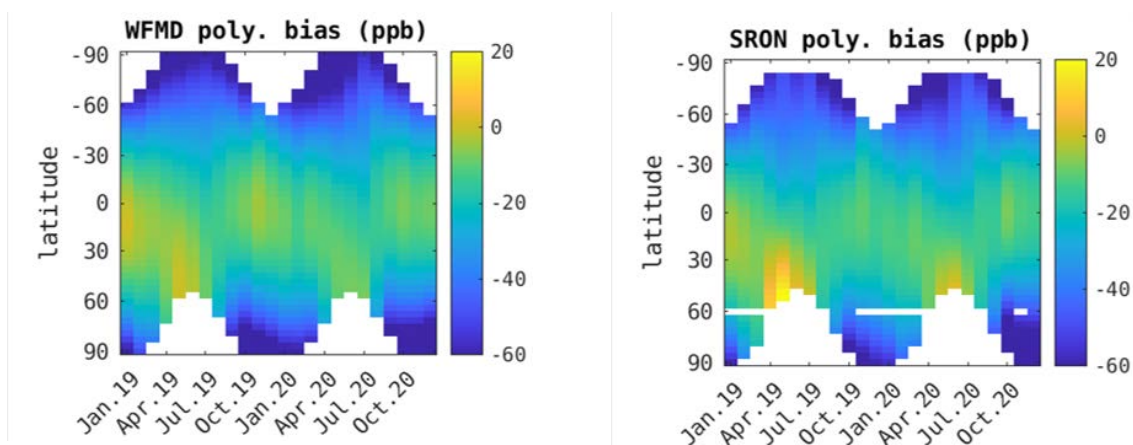


Figure 8: Second-order polynomial bias correction shown for 2019 and 2020 for CH₄_SSP_WMFD (left) and CH₄_SSP_SRONt (right), showing the extension for July-December 2020, based on the mean offset for those months in 2018 and 2019.

4.3. Methane inversion experiments with the Jena CarboScope


4.3.1. Method

After applying the bias corrections to the measurements, aggregated into super-observations, all three TROPOMI XCH₄ retrieval products were assimilated into the Jena CarboScope inversion system to attain optimized fluxes. The satellite data were assimilated alone, without combining them with other observations, in order to focus on the signals inherent to the measurements. From a scientific point of view this may not be the optimal approach: including continuous high-precision surface measurements can have a stabilizing effect on the results, but the goal of this assessment is to examine the retrieval products on their own merit.

The fluxes inferred from these satellite inversions are compared to the inversion over the same time period using the 31 flask sites, as described previously. While this is a limited station set for a surface-based global inversion, there are only a limited number of surface sites that already had quality-checked data available into mid-2020 at that point.

Comparisons are made to: (i) data-driven estimates of mean global surface concentration and the resultant calculated growth rate, (ii) grid-point annual total fluxes, and (iii) year-on-year differences for the three years for the TROPOMI products.

The GOSAT-2 products were not considered further in the inversions. Although 18 months of data were available, the record started in February 2019, and do not cover a full calendar year. A technical limitation of the Jena CarboScope is that inversions must always begin in January of a given year, though they can end at the end of any month. Thus, it was not feasible to carry out an inversion based on these data alone.

	ESA Climate Change Initiative (CCI+) Climate Assessment Report (CAR) for Climate Research Data Package 7 (CRDP#7) of the Essential Climate Variable (ECV) Greenhouse Gases (GHG)	Page 30
		Version 1.1
		20 March 2023

4.3.2. Global mean atmospheric mixing ratio and growth rate

Similar to the approach for CO₂ in Section 3.3.2, the results from the inversions are compared to global estimates derived directly from the flask measurements. In this case, two estimates are used: NOAA estimates the monthly mean global concentration of methane near the surface based on measurements from its network of marine boundary layer sites (ref: *Ed Dlugokencky, NOAA/GML* www.esrl.noaa.gov/gmd/ccgg/trends_ch4/). Similarly, the World Data Centre for Greenhouse Gas Measurements (WDCGG) provides a similar monthly measurement based on near-surface measurements, but includes more continental sites in their estimate, which leads to slightly higher estimates than NOAA's. The WDCGG estimates are reported in the annual WMO Greenhouse Gas Bulletin, and are regularly updated on the WDCGG website (https://gaw.kishou.go.jp/publications/global_mean_mole_fractions). Given the short time period available for the CRDP methane datasets being considered in the CAR, an analysis of monthly concentrations is attractive, even though we would expect this quantity to be less robust than an annual value.

To compare these to the optimized fields resulting from the inversion of the different products, the mean methane mixing ratio for each month is taken, averaged at the lowest model level over the whole globe, weighted by the area of the gridbox. The result of this comparison is shown in Figure 9. For reference, the concentrations resulting from the prior flux is included as well.

All the datasets show a similar seasonality, though the trend in the prior is negative. Most of the inversions show the typical double peak of the seasonal cycle, although it is only found in the NOAA estimate and not that of WDCGG. An offset between WDCGG and NOAA is as expected, as the former includes continental sites and not only marine background stations, and almost all methane emissions are on land. The agreement between the different inversions is good, although there are a few differences that stand out. The WFMD inversion is substantially higher than the others in December 2018, for example, but in general the WFMD XCH₄ retrievals have higher values than the SRON retrievals, so a general offset can also be seen.

Over the last six months of 2021, the near-surface concentrations deduced from the satellite retrievals grow less quickly than what is measured by the near-surface stations (NOAA and WDCGG). The reason for this is not entirely clear. This could be related to the extrapolation of the bias correction (discussed in Section 4.2.2.2 and shown in Figure 8), but could also be an edge effect of the inversion. The prior fluxes certainly do not match the general global trend, and the inversion may struggle to increase the prior fluxes sufficiently. Nonetheless, the WFMD product appears to best match the observed concentrations towards the end of the study period.

Climate Assessment Report (CAR) for Climate Research Data Package 7 (CRDP#7)

Version 1.1

of the Essential Climate Variable (ECV)
Greenhouse Gases (GHG)

20 March 2023

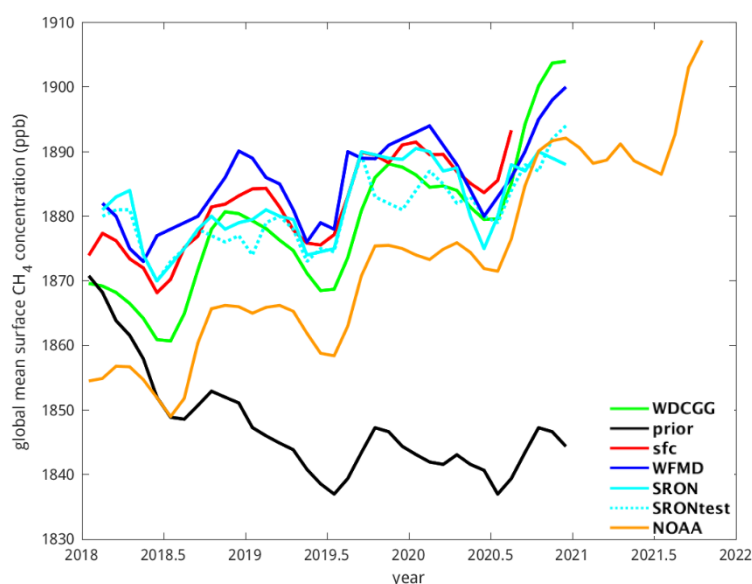


Figure 9: Monthly global mean surface CH₄ mixing ratio at the surface, based directly on in situ measurements (for NOAA in orange and WDCGG in green) or from forward simulations of the prior (in black) or optimized fluxes. The optimized fluxes are in turn constrained by different measurements, namely the surface network ("sfc", in red), CH₄_S5P_WFMD ("WFMD", in blue), CH₄_S5P_SRON ("SRON", the cyan solid line) or CH₄_S5P_SRONt ("SRONtest", the cyan dashed line).

4.3.3. Maps of annual budgets

To assess the spatial patterns inferred from the different inversions, the spatial pattern of the mean annual fluxes for 2018 are compared in Figure 11. As for the CO₂ inversions, the flux increments and the inferred gradients are much stronger for the satellite-based inversions than the surface-based inversion. This is partly the result of the increased data density: the surface-based inversion is constrained by only 31 sites, some of whose records did not even extend until the end of the inversion period. However, it can also be the result of the model trying to fit unrealistic gradients in measurements.

What is encouraging: all inversions agree on the direction and location of some flux increments, such as the decrease of the prior emissions over China and an increase over the Middle East and Central Asia. These are generally plausible results and have been emerged from other studies as well. All inversions also show a negative increment in the fluxes over Boreal North America, while only the surface-based inversion and the SRON inversions show increases over the southeast United States.

There is less clarity over the Tropics: all inversions show increased emissions over Indonesia, and the TROPOMI-based inversions show a general shift in the pattern of fluxes in the Amazon, leading to higher emissions close to the Atlantic Coast and lower emissions to the south and west. In Africa there is less consensus, though all simulations suggest large increments in the Congo Basin, a region of high uncertainty and large gradients, thanks to its proximity to the ITCZ.

Climate Assessment Report (CAR) for Climate Research Data Package 7 (CRDP#7)

Version 1.1

of the Essential Climate Variable (ECV)
Greenhouse Gases (GHG)

20 March 2023

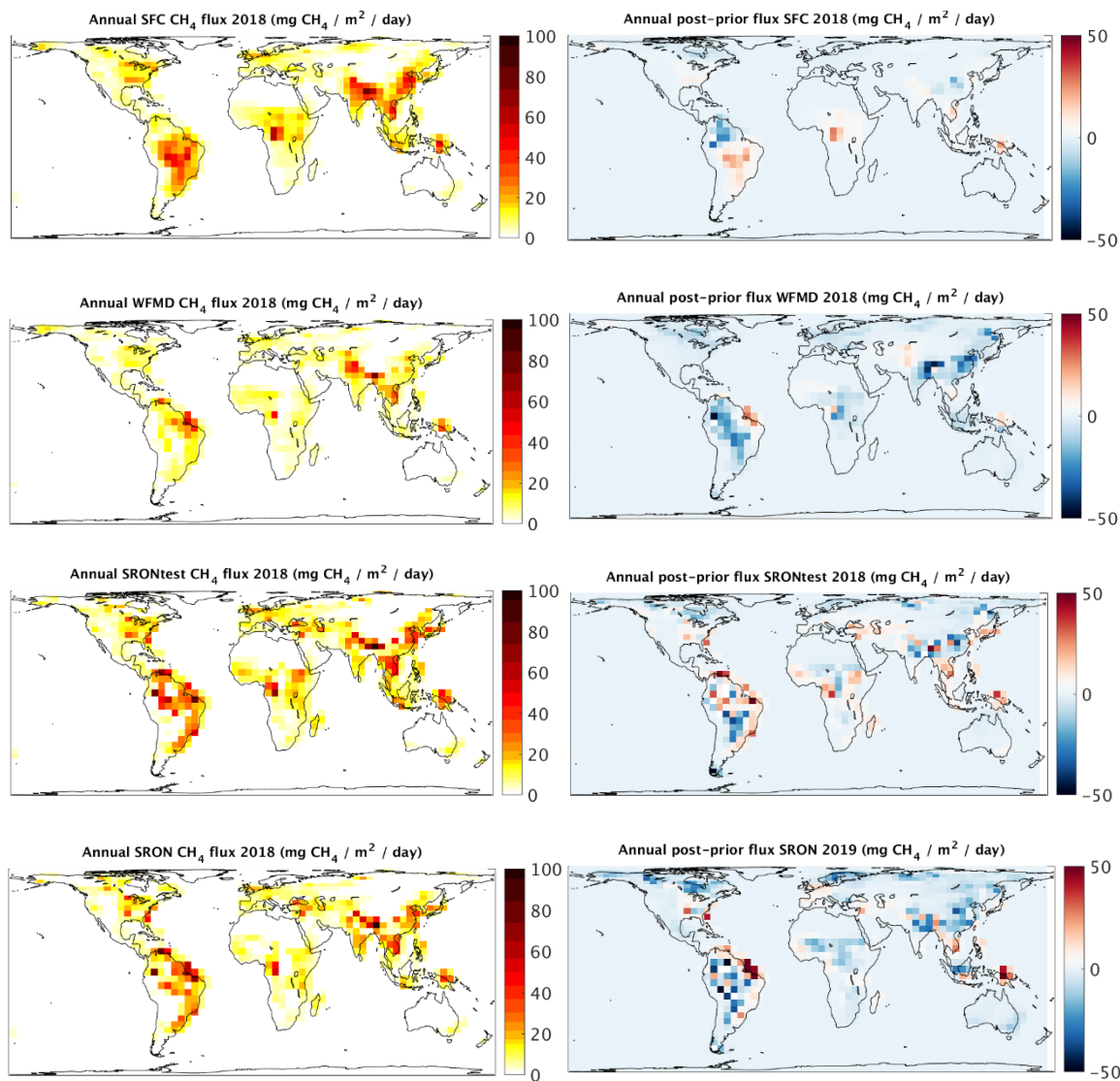


Figure 10, left side: annual flux maps for 2018 for the four inversions, from top to bottom: based on flask data, based on CH₄_S5P_WFMD, based on CH₄_S5P_SRONt, based on CH₄_S5P_SRON. The right side shows the increment compared to the prior for the same simulations.

Climate Assessment Report (CAR) for Climate Research Data Package 7 (CRDP#7)

Version 1.1

of the Essential Climate Variable (ECV)
Greenhouse Gases (GHG)

20 March 2023

4.3.4. Year-on-year flux increments

Whereas the previous section compared the flux increments to the prior, here the increments year-over-year are compared for the three TROPOMI retrievals, shown in Figure 11. (The surface-based inversion is not included, as it does not cover all of 2020.) All three satellite inversions show a general increase in the tropical methane emissions in 2019 compared to 2018, though the signal is quite a lot noisier in the two SRON retrievals. From 2019 to 2020, the SRON retrievals continue to show an increase in the Tropics, but this is not seen as clearly in the WFMD-based inversion. All three products result in an increase in high-latitude emissions in 2020 compared to 2019.

The increase in the methane growth rate in 2020 has been attributed by another study to increased wetland emissions, due to warm, wet conditions in the Northern Hemisphere, coupled with a decreased atmospheric sink (Peng et al., 2022). This study was performed using GOSAT data, but the increased high latitude fluxes seen particularly in the SRON retrievals are broadly consistent with these findings.

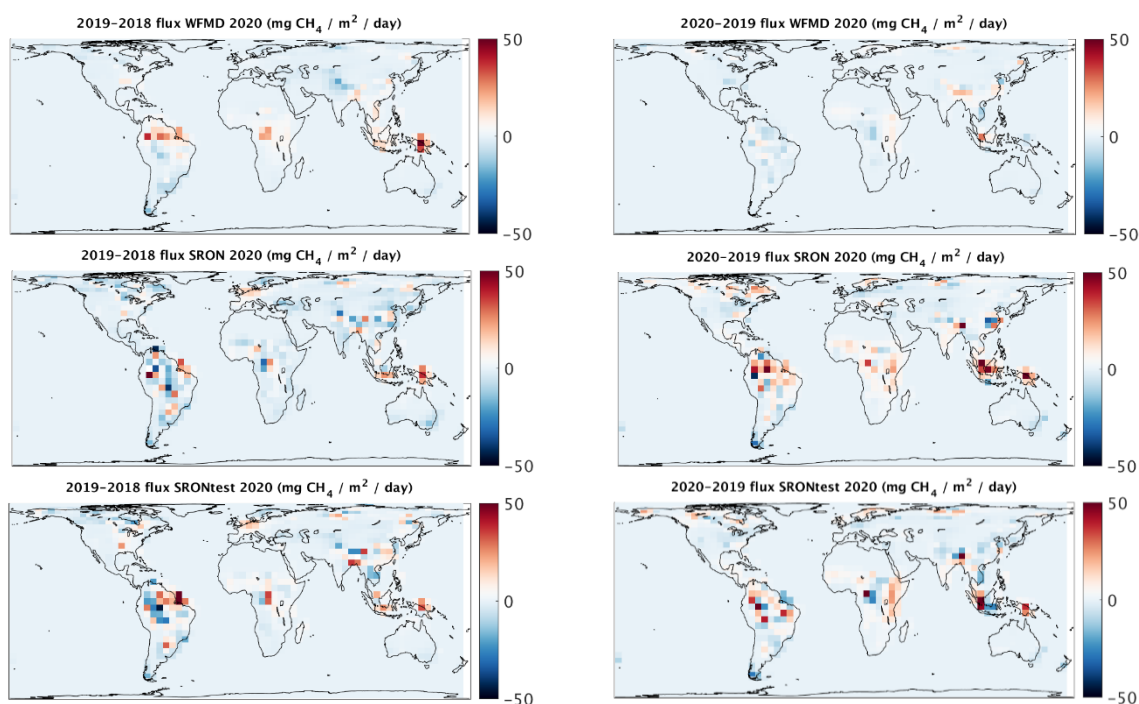


Figure 11: The year-on-year flux differences from 2018 to 2019 (left column) and from 2019 to 2020 (right column), for inversions using CH4_S5P_WFMD (top row), CH4_S5P_SRON (middle row) and CH4_S5P_SRONt (bottom row).

4.3.5. Comparison with aircraft data and TCCON

Both aircraft-based and total column TCCON measurements of XCH_4 are used to assess the performance of the different inversions. None of the measurements used here were assimilated in the inversion. Given the shorter time period of the methane inversions naturally there are less data sets available, but the approach is similar.

The comparison to the aircraft data, in Figure 12, shows that the surface-based inversion performs somewhat better than the satellite-based inversions, with on average lower bias and a smaller standard deviation, especially for mid-latitude sites. The worst performance for all inversions is for the aircraft measurements from Southern Great Plains, with a consistent low bias and very high standard deviation, likely due to the large amounts of oil and gas emissions in the region (Oklahoma, USA), leading to high variability which the coarse global model is unable to reproduce.

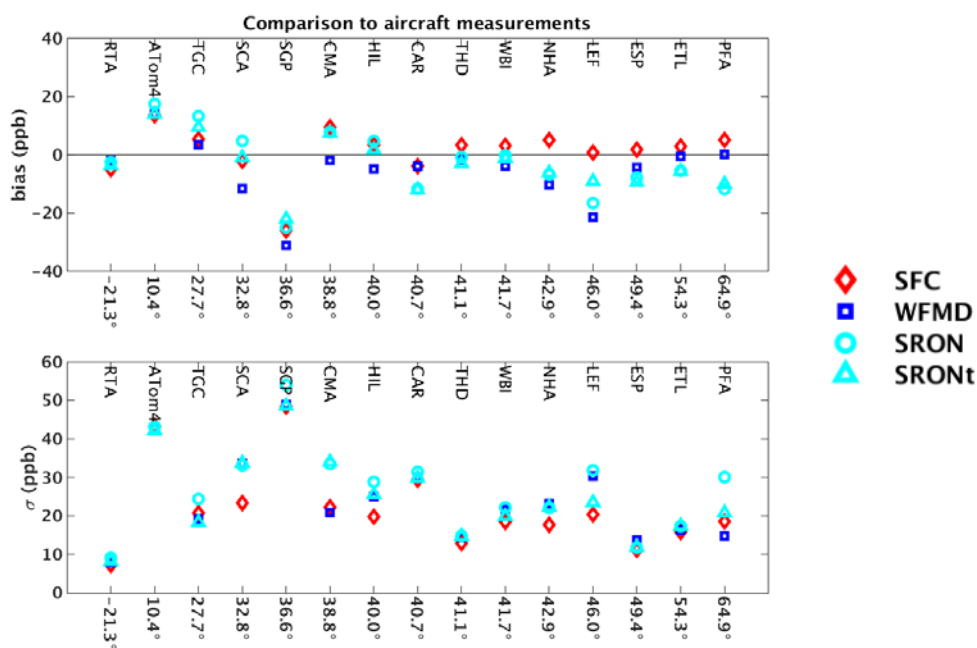


Figure 12: Comparison of optimized concentration fields to aircraft measurements, with mean bias (top panel) and standard deviation of the difference (bottom panel). The campaigns are sorted by latitude.

Climate Assessment Report (CAR) for Climate Research Data Package 7 (CRDP#7)

Version 1.1

of the Essential Climate Variable (ECV)
Greenhouse Gases (GHG)

20 March 2023

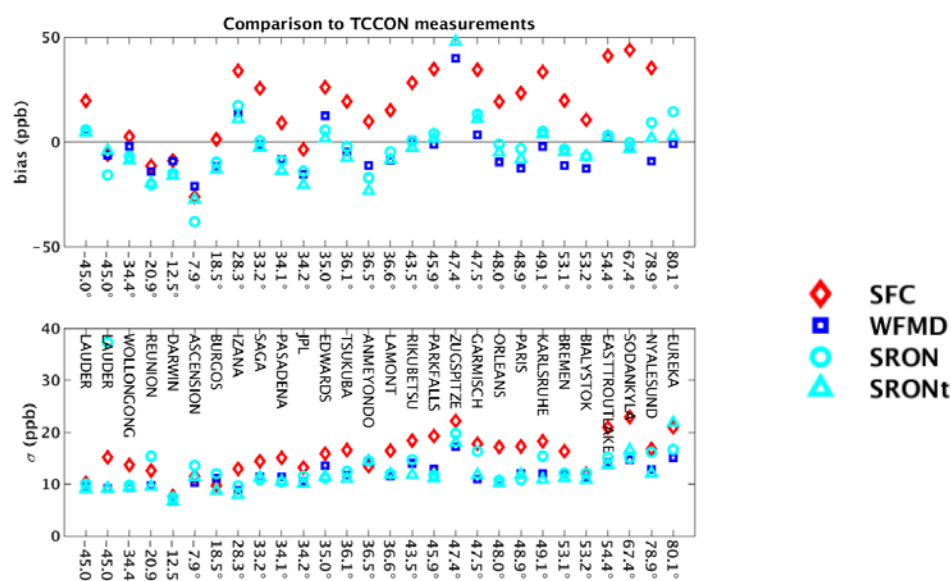



Figure 13: Comparison of optimized concentration fields from different inversions to TCCON total column measurements, with mean bias (top panel) and standard deviation of the difference (bottom panel). The stations are sorted by latitude. The station names are omitted from the upper panel for clarity. The station Lauder is listed twice, as the instrument was replaced during this period, and installed at a slightly different location. The two records overlap slightly in time.

High biases are also found for the ATom4 flight campaign, which are related to a poor representation of the position of the tropopause. The data were not filtered to include only mid-tropospheric values, as was done for the CO₂ comparison, and this flight campaign includes extremely high profiles. There is no clear evidence for an interhemispheric or latitude-dependent bias, but the measurements are also almost exclusively in the northern hemisphere.

The comparison to TCCON measurements is shown in Figure 13. Contrary to the aircraft data, the concentration fields from the satellite-based inversions clearly agree with the measurements better than those from the surface-based inversion. Both the bias and the standard deviation are consistently smaller. This is not unexpected: a bias-correction was added to the satellite products to make them consistent with the surface-based inversion, which already indicates a model-specific inconsistency between the surface concentrations and the total column concentrations. And while TCCON data are not used directly to bias-correct the current generation of satellite retrievals, they are still employed as a quality check to ensure general consistency. As such a solution to the inversion problem that minimizes the model-data mismatch to the satellite columns is also expected to agree well with the independent total column measurements of TCCON.

At the same time, the good agreement suggests that there is no significant drift of the measurements over time, for example. Zugspitze, a mountain site, shows poor agreement, which can be attributed to representation errors of the total column due to the high altitude.

	ESA Climate Change Initiative (CCI+) Climate Assessment Report (CAR) for Climate Research Data Package 7 (CRDP#7) of the Essential Climate Variable (ECV) Greenhouse Gases (GHG)	Page 36
		Version 1.1
		20 March 2023


In the comparisons with the independent aircraft-based and TCCON data, there is no single satellite product which clearly performs best. While there are some gaps towards the end of the data record for CH4_S5P_SRON due to the cloud screening procedure, most of the available TCCON time series ended before this period, and as such did not affect the outcome of this comparison.

4.3.6. Conclusions

The fluxes produced by assimilating the various TROPOMI XCH₄ products into the Jena CarboScope show some general structural agreement with each other, but diverge significantly from the fluxes based on the assimilation of surface-based measurements. While the satellite-based fluxes are better able to match the (mostly) independent TCCON total column measurements, the surface-based inversion does slightly better in reproducing independent aircraft measurements. This analysis of the resultant fields with independent data does not show that any one retrieval product clearly outperforms the others, at least on the metrics considered here. The broader spatial coverage of the CH4_S5P_WFMD retrieval, including (consistent) retrievals over the oceans, makes it an attractive product for analysis. It also reports more realistic measurement uncertainties, which have been inflated to match the observed performance compared to TCCON. Because the SRON products have such low reported measurement errors, the model may attempt to overfit noisy measurements, leading to unrealistically variable fluxes.

Despite the general agreement that is seen in concentration space, the temporal and spatial variability of the fluxes that arise from the assimilation of TROPOMI XCH₄ are not always consistent with our understanding of the methane budget and the expected variability of the fluxes driving it. The resultant variability is extremely high in both space and time, especially for the SRON retrievals, leading to unrealistically large seasonal cycles for several regions. These differences are in some ways exaggerated by the experimental setup: the XCH₄ products were assimilated alone, without including the stabilizing influence of simultaneously assimilated surface measurements. Because the spatial coverage of the measurements has such a strong seasonal cycle, small systematic errors, especially at high latitude, or in regions with high prior uncertainties, like the Tropics, may lead to significantly biased results.


Despite these concerns, the amount of detailed information about local methane gradients in these products is extraordinary, and the products have already been used extensively to analyze point sources and local-scale gradients. They are also able to well reproduce global mean mixing ratios over the three years considered in this report. However, for their application in global inversion modelling to analyse regional scale fluxes over seasonal and interannual scales, care needs to be taken to ensure that (perhaps small) systematic errors do not bias the resultant fluxes.

	ESA Climate Change Initiative (CCI+)		Page 37
	Climate Assessment Report (CAR) for Climate Research Data Package 7 (CRDP#7)		
	of the Essential Climate Variable (ECV) Greenhouse Gases (GHG)		Version 1.1
			20 March 2023

Acknowledgements

F. Chevallier thanks M. Reuter and M. Buchwitz for constructive discussions about the use and the evaluation of these products. He is very grateful to the many people involved in the air-sample measurements and in the archiving of these data. Some of the computations of Sections 3.2 and 3.3 have been performed using HPC resources from CCRT under the allocation A0090102201 made by GENCI (Grand Equipement National de Calcul Intensif). The OCO-2 ACOS data have been obtained from <http://co2.jpl.nasa.gov>. They were produced by the OCO-2 project at the Jet Propulsion Laboratory, California Institute of Technology. CAMS data are publicly available from <http://atmosphere.copernicus.eu/>.

J. Marshall acknowledges the use of computing resources of the Deutsches Klimarechenzentrum (DKRZ) granted by its Scientific Steering Committee (WLA) under project ID bd1231.

	ESA Climate Change Initiative (CCI+) Climate Assessment Report (CAR) for Climate Research Data Package 7 (CRDP#7) of the Essential Climate Variable (ECV) Greenhouse Gases (GHG)	Page 38
		Version 1.1
		20 March 2023

References

Note:

- **Links to pdf versions of all GHG-CCI+ CRDP documents are available on the GHG-CCI+ key documents website: <https://climate.esa.int/en/projects/ghgs/key-documents/>**
- **Links to pdf versions of all GHG-CCI+ publications are available on the GHG-CCI+ publications website: <https://climate.esa.int/en/projects/ghgs/publications/>**

Alexe, M., P. Bergamaschi, A. Segers, et al., Inverse modeling of CH₄ emissions for 2010–2011 using different satellite retrieval products from GOSAT and SCIAMACHY, *Atmos. Chem. Phys.*, 15, 113–133, doi:10.5194/acp-15-113-2015, 2015.

Bastos, A., Running, S.W., Gouveia, C. and Trigo, R.M: The global NPP dependence on ENSO: La-Nina and the extraordinary year of 2011. *J. Geophys. Res.* 118, 1247–1255, 2013

Basu, S., Guerlet, S., Butz, A., et al., Global CO₂ fluxes estimated from GOSAT retrievals of total column CO₂, *Atmos. Chem. Phys.*, 13, 8695–8717, 2013.

Basu, S., Krol, M., Butz, A., et al., The seasonal variation of the CO₂ flux over Tropical Asia estimated from GOSAT, CONTRAIL and IASI, *Geophys. Res. Lett.*, doi: 10.1002/2013GL059105, 2014.


Bergamaschi, P., C. Frankenberg, J. F. Meirink, M. Krol, M. G. Villani, S. Houweling, F. Dentener, E. J. Dlugokencky, J. B. Miller, L. V. Gatti, A. Engel, and I. Levin: Inverse modeling of global and regional CH₄ emissions using SCIAMACHY satellite retrievals, *J. Geophys. Res.*, 114, doi:10.1029/2009JD012287, 2009.

Bergamaschi, P., et al.: Inverse modeling of European CH₄ emissions 2001–2006, *J. Geophys. Res.*, 115(D22309), doi:10.1029/2010JD014180, 2010.

Bergamaschi, P., S. Houweling, A. Segers, M. Krol, C. Frankenberg, R. A. Scheepmaker, E. Dlugokencky, S. Wofsy, E. Kort, C. Sweeney, T. Schuck, C. Brenninkmeijer, H. Chen, V. Beck and C. Gerbig, Atmospheric CH₄ in the first decade of the 21st century: Inverse modeling analysis using SCIAMACHY satellite retrievals and NOAA surface measurements, *J. Geophys. Res.*, 118, doi:10.1002/jgrd.50480, 2013.

Bloom, A. A., Palmer, P. I., Fraser, A., and Reay, D. S.: Seasonal variability of tropical wetland CH₄ emissions: the role of the methanogen-available carbon pool, *Biogeosciences*, 9, 2821–2830, doi:10.5194/bg-9-2821-2012, 2012

Boden, T. A., Marland, G., and Andres, R. J.: Global, regional, and national fossil-fuel CO₂ emissions. Carbon Dioxide Information Analysis Center, Oak Ridge National Laboratory, U.S. Department of Energy, Oak Ridge, Tenn., U.S.A., Doi:10.3334/CDIAC/00001_V2013, 2013

	ESA Climate Change Initiative (CCI+) Climate Assessment Report (CAR) for Climate Research Data Package 7 (CRDP#7) of the Essential Climate Variable (ECV) Greenhouse Gases (GHG)	Page 39
		Version 1.1
		20 March 2023

Buchwitz, M., M. Reuter, O. Schneising, et al., The Greenhouse Gas Climate Change Initiative (GHG-CCI): comparison and quality assessment of near-surface-sensitive satellite-derived CO₂ and CH₄ global data sets, *Remote Sensing of Environment*, 162, 344–362, doi:10.1016/j.rse.2013.04.024, 2015.

Buchwitz, M., M. Reuter, O. Schneising, W. Hewson, R.G. Detmers, H. Boesch, O.P. Hasekamp, I. Aben, H. Bovensmann, J.P. Burrows, A. Butz, F. Chevallier, B. Dils, C. Frankenberg, J. Heymann, G. Lichtenberg, M. De Mazière, J. Notholt, R. Parker, T. Warneke, C. Zehner, D.W.T. Griffith, N.M. Deutscher, A. Kuze, H. Suto, D. Wunch, 2017: Global satellite observations of column-averaged carbon dioxide and methane: The GHG-CCI XCO₂ and XCH₄ CRDP3 data set, *Remote Sensing of Environment*, 203, 276-295, doi:dx.doi.org/10.1016/j.rse.2016.12.027.

Buchwitz, M., Dils, B., Reuter, M., Schneising, O., Hilker, M., Preval, S., Boesch, H., Borsdoff, T., Landgraf, J., Krisna, T.C., Product Validation and Intercomparison Report (PVIR) for the Essential Climate Variable (ECV) Greenhouse Gases (GHG): XCO₂ and/or XCH₄ from OCO-2, TanSat, Sentinel-5-Precursor and GOSAT-2, v3.0, 16 February 2022, 2022.

Butz, A., Guerlet, S., Hasekamp, O., et al., Toward accurate CO₂ and CH₄ observations from GOSAT, *Geophys. Res. Lett.*, doi:10.1029/2011GL047888, 2011.

Canadell, J. G., Ciais, P., Dhakal, S., et al., Interactions of the carbon cycle, human activity, and the climate system: a research portfolio, *Curr. Opin. Environ. Sustainabil.*, 2, 301–311, 2010.

Chevallier, F., et al.: Inferring CO₂ sources and sinks from satellite observations: method and application to TOVS data. *J. Geophys. Res.*, 110, D24309, 2005.


Chevallier, F.: Impact of correlated observation errors on inverted CO₂ surface fluxes from OCO measurements, *Geophys. Res. Lett.*, 34, L24804, doi:10.1029/2007GL030463, 2007.

Chevallier, F., Maksyutov, S., Bousquet, P., Bréon, F.-M., Saito, R., Yoshida, Y., and Yokota, T.: On the accuracy of the CO₂ surface fluxes to be estimated from the GOSAT observations. *Geophys. Res. Lett.*, 36, L19807, doi:10.1029/2009GL040108, 2009.

Chevallier, F., et al.: CO₂ surface fluxes at grid point scale estimated from a global 21-year reanalysis of atmospheric measurements. *J. Geophys. Res.*, 115, D21307, doi:10.1029/2010JD013887, 2010a.

Chevallier, F., Feng, L., Boesch, H., Palmer, P., and Rayner, P.: On the impact of transport model errors for the estimation of CO₂ surface fluxes from GOSAT observations. *Geophys. Res. Lett.*, 37, L21803, doi:10.1029/2010GL044652, 2010b.

Chevallier, F., Deutscher, N. M., Conway, T. J., Ciais, P., Ciattaglia, L., Dohe, S., Frohlich, M., Gomez-Pelaez, A. J., Griffith, D., Hase, F., Haszpra, L., Krummel, P., Kyro, E., Labuschagne, C., Langenfelds, R., Machida, T., Maignan, F., Matsueda, H., Morino, I., Notholt, J., Ramonet, M., Sawa, Y., Schmidt, M., Sherlock, V., Steele, P., Strong, K., Sussmann, R., Wennberg, P., Wofsy, S., Worthy, D., Wunch, D., and

	ESA Climate Change Initiative (CCI+) Climate Assessment Report (CAR) for Climate Research Data Package 7 (CRDP#7) of the Essential Climate Variable (ECV) Greenhouse Gases (GHG)	Page 40
		Version 1.1
		20 March 2023

Zimnoch, M.: Global CO₂ fluxes inferred from surface air-sample measurements and from TCCON retrievals of the CO₂ total column, *Geophys. Res. Lett.*, 38, L24810, doi:10.1029/2011GL049899, 2011

Chevallier, F., Bergamaschi, P., Kaminiski, T., Scholze, M., Climate Assessment Report (CAR) for the GHG-CCI project of ESA's Climate Change Initiative, version 1.1 (CARv1.1), 18. Nov. 2013, 2013.

Chevallier, F., and O'Dell, C. W., Error statistics of Bayesian CO₂ flux inversion schemes as seen from GOSAT, *Geophys. Res. Lett.*, doi: 10.1002/grl.50228, 2013.

Chevallier, F., Palmer, P.I., Feng, L., Boesch, H., O'Dell, C.W., Bousquet, P., Towards robust and consistent regional CO₂ flux estimates from in situ and space-borne measurements of atmospheric CO₂, *Geophys. Res. Lett.*, 41, 1065-1070, DOI: 10.1002/2013GL058772, 2014a.

Chevallier, F., Buchwitz, M., Bergamaschi, et al., User Requirements Document for the GHG-CCI project of ESA's Climate Change Initiative, version 2 (URDv2), 28. August 2014, 2014b.

Chevallier, F.: On the statistical optimality of CO₂ atmospheric inversions assimilating CO₂ column retrievals, *Atmos. Chem. Phys.*, 15, 11133–11145, <https://doi.org/10.5194/acp-15-11133-2015>, 2015.

Chevallier, F., P. Bergamaschi, D. Brunner, S. Gonzi, S. Houweling, T. Kaminski, G. Kuhlmann, T. T. van Leeuwen, J. Marshall, P. I. Palmer, and M. Scholze, Climate Assessment Report for the GHG-CCI project of ESA's Climate Change Initiative, pp. 87, version 2, 22 April 2015, 2015.

Chevallier, F., M. Alexe, P. Bergamaschi, D. Brunner, L. Feng, S. Houweling, T. Kaminski, W. Knorr, T. T. van Leeuwen, J. Marshall, P. I. Palmer, M. Scholze, A.-M. Sundström and M. Voßbeck, Climate Assessment Report for the GHG-CCI project of ESA's Climate Change Initiative, pp. 94, version 3, 3 May 2016, 2016.


Chevallier, F., P. Bergamaschi, D. Brunner, L. Feng, S. Houweling, T. Kaminski, W. Knorr, J. Marshall, P. I. Palmer, S. Pandey, M. Reuter, M. Scholze, and M. Voßbeck, Climate Assessment Report for the GHG-CCI project of ESA's Climate Change Initiative, pp. 96, version 4,, 27 March 2017, 2017.

Chevallier, F., Remaud, M., O'Dell, C. W., Baker, D., Peylin, P., and Cozic, A.: Objective evaluation of surface- and satellite-driven carbon dioxide atmospheric inversions, *Atmos. Chem. Phys.*, 19, 14233–14251, <https://doi.org/10.5194/acp-19-14233-2019>, 2019.

Chevallier, F., Climate Assessment Report for the GHG-CCI+ project of ESA's Climate Change Initiative, pp. 36, version 1.2, 20 March 2020, 2020.

Chevallier, F. and Marshall, J., Climate Assessment Report for the GHG-CCI+ project of ESA's Climate Change Initiative, pp. 59, version 2.0, 9 March 2021, 2021.

Chevallier, F., Validation report for the inverted CO₂ fluxes, v20r2. CAMS deliverable CAMS73_2018SC2_D73.1.4.1-2020-v5_202109. <http://atmosphere.copernicus.eu/>, 2021a.

	ESA Climate Change Initiative (CCI+) Climate Assessment Report (CAR) for Climate Research Data Package 7 (CRDP#7) of the Essential Climate Variable (ECV) Greenhouse Gases (GHG)	Page 41
		Version 1.1
		20 March 2023

Chevallier, F., Evaluation and Quality control document for the OCO-2-driven CO₂ inversion FT20r3. CAMS deliverable CAMS73_2018SC2_D73.4.2.2-2021-v1_202104. <http://atmosphere.copernicus.eu/>, 2021b.

Cogan, A. J., Boesch, H., Parker, R. J., et al., Atmospheric carbon dioxide retrieved from the Greenhouse gases Observing SATellite (GOSAT): Comparison with ground-based TCCON observations and GEOS-Chem model calculations, *J. Geophys. Res.*, 117, D21301, doi:10.1029/2012JD018087, 2012.

Conway, T. J., Tans, P. P., Waterman, L. S., Thoning, K. W., Kitzis, D. R., Masarie, K. A. and Zhang, N.: Evidence for interannual variability of the carbon cycle from the National Oceanic and Atmospheric Administration/Climate Monitoring and Diagnostics Laboratory Global Air Sampling Network, *J. Geophys. Res.*, 99(D11), 22,831–22,855, doi:10.1029/94JD01951, 1994

Cramer, W., Kicklighter, D. W., Bondeau, A., Iii, B. M., Churkina, G., Nemry, B., Ruimy, A., Schloss, A. L. and Intercomparison, ThE. P. OF. ThE. P. NpP. M., Comparing global models of terrestrial net primary productivity (NPP): overview and key results. *Global Change Biology*, 5: 1–15. doi:10.1046/j.1365-2486.1999.00009.x, 1999.

Cressot, C., F. Chevallier, P. Bousquet, et al., On the consistency between global and regional methane emissions inferred from SCIAMACHY, TANSO-FTS, IASI and surface measurements, *Atmos. Chem. Phys.*, 14, 577-592, 2014.

Cressot, C., Pison, I., Rayner, P. J., Bousquet, P., Fortems-Cheiney, A., and Chevallier, F.: Can we detect regional methane anomalies? A comparison between three observing systems, *Atmos. Chem. Phys.*, 16, 9089-9108, doi:10.5194/acp-16-9089-2016, 2016.


Crevoisier, C., Sweeney, C., Gloor, M., Sarmiento, J. L., and Tans, P. P.: Regional U.S. carbon sinks from three-dimensional atmospheric CO₂ sampling, *Proc. Natl. Acad. Sci.* (2010), 107: 18348-18353, 2010.

Crowell, S., Baker, D., Schuh, A., Basu, S., Jacobson, A. R., Chevallier, F., Liu, J., Deng, F., Feng, L., McKain, K., Chatterjee, A., Miller, J. B., Stephens, B. B., Eldering, A., Crisp, D., Schimel, D., Nassar, R., O'Dell, C. W., Oda, T., Sweeney, C., Palmer, P. I., and Jones, D. B. A.: The 2015–2016 carbon cycle as seen from OCO-2 and the global in situ network, *Atmos. Chem. Phys.*, 19, 9797–9831, <https://doi.org/10.5194/acp-19-9797-2019>, 2019.

Dee, D. P., et al., The ERA-Interim reanalysis: configuration and performance of the data assimilation system, *Q. J. R. Meteorol. Soc.*, 137, 553–597, 2011.

Desroziers G., Berre, L., Chapnik, B., and Poli, P.: Diagnosis of observation, background and analysis error statistics in observation space. *Q. J. Roy. Meteor. Soc.*, 131, 3385-3396, 2005.

Detmers, R., Hasekamp, O., Aben, I., Houweling, S., van Leeuwen, T.T., Butz, A., Landgraf, J., Kohler, P., Guanter, L., and Poulter, B.: Anomalous carbon uptake in Australia as seen by GOSAT. *Geophysical Research Letters*, 42(19), 2015

	ESA Climate Change Initiative (CCI+)		Page 42
	Climate Assessment Report (CAR) for Climate Research Data Package 7 (CRDP#7)		Version 1.1
			20 March 2023
	of the Essential Climate Variable (ECV) Greenhouse Gases (GHG)		

Dlugokencky, E. J., L. P. Steele, P. M. Lang, and K. A. Masarie, The growth rate and distribution of atmospheric methane, *J. Geophys. Res.*, 99, 17021–17043, 1994.

Dlugokencky, E. J., S. Houweling, L. Bruhwiler, K. A. Masarie, P.M. Lang, J. B. Miller, and P. P. Tans, Atmospheric methane levels off: Temporary pause or a new steady-state? *Geophys. Res. Lett.*, 30(19), 1992, doi:10.1029/2003GL018126, 2003.

Dlugokencky, E. J., Bruhwiler, L., White, J. W. C., et al., Observational constraints on recent increases in the atmospheric CH₄ burden, *Geophys. Res. Lett.*, 36, L18803, doi:10.1029/2009GL039780, 2009.

Dlugokencky, E., P. Lang, J. Mund, A. Croswell, M. Croswell, and K. Thoning, Atmospheric carbon dioxide dry air mole fractions from the NOAA ESRL carbon cycle cooperative global air sampling network, 1968-2015, 2016.

Dubovik, O. and King, M. D.: A flexible inversion algorithm for retrieval of aerosol optical properties from Sun and sky radiance measurements, *J. Geophys. Res.*, 105, 20673–20696, 2000.

Enting, I. G.: Inverse Problems in Atmospheric Constituent Transport. Cambridge University Press, 2002.

ESA: A-SCOPE - Advanced Space Carbon and Climate Observation of Planet Earth, Technical Report SP-1313/1, European Space Agency, Noordwijk, The Netherlands. 2008


Feng, L., Palmer, P. I., Bösch, H., and Dance, S.: Estimating surface CO₂ fluxes from space-borne CO₂ dry air mole fraction observations using an ensemble Kalman Filter, *Atmos. Chem. Phys.*, 9, 2619–2633, doi:10.5194/acp-9-2619-2009, 2009.

Feng, L., P. I. Palmer, R. J. Parker, et al., Estimates of European uptake of CO₂ inferred from GOSAT X_{CO2} retrievals: sensitivity to measurement bias inside and outside Europe, *Atmos. Chem. Phys.*, 16, 1289–1302, doi:10.5194/acp-16-1289-2016, 2016a.

Feng, L., Palmer, P. I., Bösch, H., Parker, R. J., Webb, A. J., Correia, C. S. C., Deutscher, N. M., Domingues, L. G., Feist, D. G., Gatti, L. V., Gloor, E., Hase, F., Kivi, R., Liu, Y., Miller, J. B., Morino, I., Sussmann, R., Strong, K., Uchino, O., Wang, J., and Zahn, A.: Consistent regional fluxes of CH₄ and CO₂ inferred from GOSAT proxy XCH₄:XCO₂ retrievals, 2010–2014, *Atmos. Chem. Phys. Discuss.*, doi:10.5194/acp-2016-868, in review, 2016b. Frankenberg, C., Aben, I., Bergamaschi, P., et al., Global column-averaged methane mixing ratios from 2003 to 2009 as derived from SCIAMACHY: Trends and variability, *J. Geophys. Res.*, doi:10.1029/2010JD014849, 2011.

Frankenberg, C., Product User Guide (PUG) for the IMAP-DOAS XCH₄ SCIAMACHY Data Products, version 1, ESA Climate Change Initiative (CCI) GHG-CCI project, 13 Dec. 2012, 2012.

Fraser, A., Palmer, P. I., Feng, L., et al., Estimating regional methane surface fluxes: the relative importance of surface and GOSAT mole fraction measurements, *Atmos. Chem. Phys.*, 13, 5697–5713, doi:10.5194/acp-13-5697-2013, 2013.

	ESA Climate Change Initiative (CCI+) Climate Assessment Report (CAR) for Climate Research Data Package 7 (CRDP#7) of the Essential Climate Variable (ECV) Greenhouse Gases (GHG)	Page 43
		Version 1.1
		20 March 2023

Fraser, A., Palmer, P. I., Feng, L. et al., Estimating regional fluxes of CO₂ and CH₄ using space-borne observations of XCH₄:XCO₂, *Atmos. Chem. Phys.*, 14, 12883-12895, doi:10.5194/acp-14-12883-2014, 2014.

Friedl, M. A., Strahler, A. H., and Hodges, J.: ISLSCP II MODIS (Collection 4) IGBP Land Cover, 2000–2001, in: ISLSCP Initiative II Collection, Data set, edited by: Hall, F. G., Collatz, G., Meeson, B., Los, S., Brown de Colstoun, E., and Landis, D., Oak Ridge National Laboratory Distributed Active Archive Center, Oak Ridge, Tennessee, USA, doi:10.3334/ORNLDAAAC/96

Friedlingstein, P., Jones, M. W., O'Sullivan, M., Andrew, R. M., Bakker, D. C. E., Hauck, J., Le Quéré, C., Peters, G. P., Peters, W., Pongratz, J., Sitch, S., Canadell, J. G., Ciais, P., Jackson, R. B., Alin, S. R., Anthoni, P., Bates, N. R., Becker, M., Bellouin, N., Bopp, L., Chau, T. T. T., Chevallier, F., Chini, L. P., Cronin, M., Currie, K. I., Decharme, B., Djeutchoang, L., Dou, X., Evans, W., Feely, R. A., Feng, L., Gasser, T., Gilfillan, D., Gkritzalis, T., Grassi, G., Gregor, L., Gruber, N., Gürses, Ö., Harris, I., Houghton, R. A., Hurtt, G. C., Iida, Y., Ilyina, T., Luijkx, I. T., Jain, A. K., Jones, S. D., Kato, E., Kennedy, D., Klein Goldewijk, K., Knauer, J., Korsbakken, J. I., Körtzinger, A., Landschützer, P., Lauvset, S. K., Lefèvre, N., Lienert, S., Liu, J., Marland, G., McGuire, P. C., Melton, J. R., Munro, D. R., Nabel, J. E. M. S., Nakaoka, S.-I., Niwa, Y., Ono, T., Pierrot, D., Poulter, B., Rehder, G., Resplandy, L., Robertson, E., Rödenbeck, C., Rosan, T. M., Schwinger, J., Schwingshackl, C., Séférian, R., Sutton, A. J., Sweeney, C., Tanhua, T., Tans, P. P., Tian, H., Tilbrook, B., Tubiello, F., van der Werf, G., Vuichard, N., Wada, C., Wanninkhof, R., Watson, A., Willis, D., Wiltshire, A. J., Yuan, W., Yue, C., Yue, X., Zaehle, S., and Zeng, J.: Global Carbon Budget 2021, *Earth Syst. Sci. Data Discuss.* [preprint], <https://doi.org/10.5194/essd-2021-386>, in review, 2021.


Gatti, L. V., Gloor, M., Miller, J. B., Doughty, C. E., Malhi, Y., Domingues, L. G., Basso, L. S., Martinewski, A., Correia, C. S. C., Borges, V. F., Freitas, S., Braz, R., Anderson, L. O., Rocha, H., Grace, J., Philips, O. L., and Lloyd, J.: Drought sensitivity of Amazonian carbon balance revealed by atmospheric measurements, *Nature*, 506(7486), 76-80, doi:10.1038/nature12957, 2014

Cooperative Global Atmospheric Data Integration Project. (2020). *Multi-laboratory compilation of atmospheric carbon dioxide data for the period 1957-2019; obspack_co2_1_GLOBALVIEWplus_v6.0_2020_09_11* [Data set]. NOAA Earth System Research Laboratory, Global Monitoring Division. <https://doi.org/10.25925/20200903>

Guerlet, S., Basu, S., Butz, A., et al., Reduced carbon uptake during the 2010 Northern Hemisphere summer from GOSAT, *Geophys. Res. Lett.*, doi: 10.1002/grl.50402, 2013.

Gurney, K.R., et al.: Towards robust regional estimates of CO₂ sources and sinks using atmospheric transport models. *Nature*, 415:6872, 626-630, 2002.

Harris, I., Jones, P.D., Osborn, T.J. and Lister, D.H., Updated high-resolution grids of monthly climatic observations – the CRU TS3.10 Dataset. *Int. J. Climatol.* doi: 10.1002/joc.3711, 2013

	ESA Climate Change Initiative (CCI+)		Page 44
	Climate Assessment Report (CAR) for Climate Research Data Package 7 (CRDP#7)		Version 1.1
			20 March 2023
	of the Essential Climate Variable (ECV) Greenhouse Gases (GHG)		

Haverd, V., Raupach, M. R., Briggs, P. R., J. G. Canadell., Davis, S. J., Law, R. M., Meyer, C. P., Peters, G. P., Pickett-Heaps, C., and Sherman, B.: The Australian terrestrial carbon budget, *Biogeosciences*, 10, 851-869, doi:10.5194/bg-10-851-2013, 2013.

Hayman, G. D., O'Connor, F. M., Dalvi, et al., Comparison of the HadGEM2 climate-chemistry model against in-situ and SCIAMACHY atmospheric methane data, *Atmos. Chem. Phys.*, 14, 13257-13280, doi:10.5194/acp-14-13257-2014, 2014.

Heimann, M.: The global atmospheric tracer model TM2, Technical Report No. 10, Max-Planck-Institut für Meteorologie, Hamburg, Germany. 1995

Heimann, M., G. Esser, A. Haxeltine, J. Kaduk, D.W. Kicklighter, W. Knorr, G. H. Kohlmaier, A. D. McGuire, J. Melillo, B. Moore, et al., Evaluation of terrestrial carbon cycle models through simulations of the seasonal cycle of atmospheric CO₂: First results of a model intercomparison study, *Global Biogeochemical Cycles*, 12, 1–24, 1998.

Heimann, M. and S. Körner: The global atmospheric tracer model TM3. In: Max-Planck-Institut für Biogeochemie (Eds.): Technical Report. Vol. 5. Max-Planck-Institut für Biogeochemie, Jena. pp. 131, 2003.


Heymann, J., Schneising, O., Reuter, M., et al., SCIAMACHY WFM-DOAS XCO₂: comparison with CarbonTracker XCO₂ focusing on aerosols and thin clouds, *Atmos. Meas. Tech.*, 5, 1935-1952, 2012.

Hourdin, F., Foujols, M.-A., Codron, F., Guemas, V., Dufresne, J.-L., Bony, S., Denvil, S., Guez, L., Lott, F., Ghattas, J., Braconnot, P., Marti, O., Meurdesoif, Y., & Bopp, L. (2013). Impact of the LMDZ atmospheric grid configuration on the climate and sensitivity of the IPSL-CM5A coupled model. *Climate Dynamics*, 40, 2167–2192. <https://doi.org/10.1007/s00382-012-1411-3>

Houweling, S., et al.: The importance of transport model uncertainties for the estimation of CO₂ sources and sinks using satellite measurements. *Atmos. Chem. Phys.*, 10, 9981-9992, doi:10.5194/acp-10-9981-2010, 2010.

Houweling, S., M. Krol, P. Bergamaschi, C. Frankenberg, E. J. Dlugokencky, I. Morino, J. Notholt, V. Sherlock, D. Wunch, V. Beck, C. Gerbig, H. Chen, E. A. Kort, T. Röckmann and I. Aben, A multi-year methane inversion using SCIAMACHY, accounting for systematic errors using TCCON measurements, *Atmos. Chem. Phys.*, 14, 3991–4012, doi:10.5194/acp-14-3991-2014, 2014.

Houweling, S., D. Baker, S. Basu, H. Boesch, A. Butz, F. Chevallier, F. Deng, E. Dlugokencky, L. Feng, A. Ganshin, O. P. Hasekamp, D. Jones, S. Maksyutov, J. Marshall, T. Oda, C. O'Dell, S. Oshchepkov, P. Paul, P. Peylin, Z. Poussi, F. Reum, H. Takagi, Y. Yoshida, R. Zhuravlev, An inter-comparison of inverse models for estimating sources and sinks of CO₂ using GOSAT measurements. *J. Geophys. Res. Atmos.*, 120, 5253–5266, doi:10.1002/2014JD022962, 2015.

	ESA Climate Change Initiative (CCI+) Climate Assessment Report (CAR) for Climate Research Data Package 7 (CRDP#7) of the Essential Climate Variable (ECV) Greenhouse Gases (GHG)	Page 45
		Version 1.1
		20 March 2023

Hu, H., Hasekamp, O., Butz, A., Galli, A., Landgraf, J., Aan de Brugh, J., Borsdorff, T., Scheepmaker, R., and Aben, I.: The operational methane retrieval algorithm for TROPOMI, *Atmos. Meas. Tech.*, 9, 5423–5440, <https://doi.org/10.5194/amt-9-5423-2016>, 2016.

Kirschke, S., Bousquet, P., Ciais, P., et al., Three decades of global methane sources and sinks, *Nat. Geosci.*, 6, 813–823, doi:10.1038/ngeo1955, 2013.

Kort, E. A., Frankenberg, C., Costigan, K. R., et al., Four corners: The largest US methane anomaly viewed from space, *Geophys. Res. Lett.*, 41, doi:10.1002/2014GL061503, 2014.

Krisna, T. C., et al.: ESA Climate Change Initiative “Plus” (CCI+) Product User Guide (PUG) Version 3.0 for the RemoTeC XCO₂ GOSAT-2 SRON Full-Physics Product (CO₂_GO₂_SRFP) Version 2.0.0, Technical Report, pp. 21, https://www.iup.uni-bremen.de/carbon_ghg/docs/GHG-CCIplus/CRDP7/PUGv3_GHG-CCI_CO2_GO2_SRFP_v2.0.0.pdf, 2022a.

Krisna, T. C., et al.: ESA Climate Change Initiative “Plus” (CCI+) Product User Guide (PUG) Version 3.0 for the RemoTeC XCH₄ GOSAT-2 PROXY Product (CH₄_GO₂_SRPR) version 2.0.0, https://www.iup.uni-bremen.de/carbon_ghg/docs/GHG-CCIplus/CRDP7/PUGv3_GHG-CCI_CH4_GO2_SRPR_v2.0.0.pdf, 2022b.


Krol, M. C., S. Houweling, B. Bregman, M. van den Broek, A. Segers, P. van Velthoven, W. Peters, F. Dentener, and P. Bergamaschi, The two-way nested global chemistry-transport zoom model TM5: algorithm and applications, *Atmos. Chem. Phys.*, 5, 417–432, 2005.

Lindqvist, H., C. W. O'Dell, S. Basu, H. Boesch, F. Chevallier, N. Deutscher, L. Feng, B. Fisher, F. Hase, M. Inoue, R. Kivi, I. Morino, P. I. Palmer, R. Parker, M. Schneider, R. Sussmann, and Y. Yoshida, Does GOSAT capture the true seasonal cycle of carbon dioxide?, *Atmos. Chem. Phys.*, 15, 13023–13040, doi:10.5194/acp-15-13023-2015, 2015.

Lorente, A., Borsdorff, T., Butz, A., Hasekamp, O., aan de Brugh, J., Schneider, A., Wu, L., Hase, F., Kivi, R., Wunch, D., Pollard, D. F., Shiomi, K., Deutscher, N. M., Velasco, V. A., Roehl, C. M., Wennberg, P. O., Warneke, T., and Landgraf, J.: Methane retrieved from TROPOMI: improvement of the data product and validation of the first 2 years of measurements, *Atmos. Meas. Tech.*, 14, 665–684, <https://doi.org/10.5194/amt-14-665-2021>, 2021.

Ma, X., A. Huete, J. Cleverly, D. Eamus, F. Chevallier, J. Joiner, B. Poulter, Y. Zhang, L. Guanter, W. Meyer, Z. Xie, G. Ponce-Campos: Drought rapidly disseminates the 2011 large CO₂ uptake in semi-arid Australia. *Scientific Reports*, 6. doi: 10.1038/srep37747, 2016.

Mäder, J. A., J. Staehelin, D. Brunner, W. A. Stahel, I. Wohltmann, and T. Peter, Statistical modeling of total ozone: Selection of appropriate explanatory variables, *J. Geophys. Res.*, 112, D11108, doi:10.1029/2006JD007694, 2007.

	ESA Climate Change Initiative (CCI+)		Page 46
	Climate Assessment Report (CAR)		
	for Climate Research Data Package 7 (CRDP#7)		Version 1.1
	of the Essential Climate Variable (ECV) Greenhouse Gases (GHG)		20 March 2023

Meirink, J. F., P. Bergamaschi, and M. Krol: Four-dimensional variational data assimilation for inverse modelling of atmospheric methane emissions: Method and comparison with synthesis inversion, *Atmos. Chem. Phys.*, 8, 6341–6353, 2008.

Monteil, G., Houweling, S., Butz, A., et al., Comparison of CH₄ inversions based on 15 months of GOSAT and SCIAMACHY observations, *J. Geophys. Res.*, doi: 10.1002/2013JD019760, Vol 118, Issue 20, 11807–11823, 2013.

O'Dell, C. W., Connor, B., Bösch, H., O'Brien, D., Frankenberg, C., Castano, R., Christi, M., Eldering, D., Fisher, B., Gunson, M., McDuffie, J., Miller, C. E., Natraj, V., Oyafo, F., Polonsky, I., Smyth, M., Taylor, T., Toon, G. C., Wennberg, P. O., and Wunch, D.: The ACOS CO₂ retrieval algorithm – Part 1: Description and validation against synthetic observations, *Atmos. Meas. Tech.*, 5, 99–121, doi:10.5194/amt-5-99-2012, 2012.

O'Dell, C. W., Eldering, A., Wennberg, P. O., Crisp, D., Gunson, M. R., Fisher, B., Frankenberg, C., Kiel, M., Lindqvist, H., Mandrake, L., Merrelli, A., Natraj, V., Nelson, R. R., Osterman, G. B., Payne, V. H., Taylor, T. E., Wunch, D., Drouin, B. J., Oyafo, F., Chang, A., McDuffie, J., Smyth, M., Baker, D. F., Basu, S., Chevallier, F., Crowell, S. M. R., Feng, L., Palmer, P. I., Dubey, M., García, O. E., Griffith, D. W. T., Hase, F., Iraci, L. T., Kivi, R., Morino, I., Notholt, J., Ohyama, H., Petri, C., Roehl, C. M., Sha, M. K., Strong, K., Sussmann, R., Te, Y., Uchino, O., and Velasco, V. A.: Improved retrievals of carbon dioxide from Orbiting Carbon Observatory-2 with the version 8 ACOS algorithm, *Atmos. Meas. Tech.*, 11, 6539–6576, <https://doi.org/10.5194/amt-11-6539-2018>, 2018.


Oda, T., and Maksyutov, S.: A very high-resolution (1 km×1 km) global fossil fuel CO₂ emission inventory derived using a point source database and satellite observations of nighttime lights, *Atmos. Chem. Phys.*, 11, 543–556, doi:10.5194/acp-11-543-2011, 2011.

Olivier, J. G. J., van Aardenne, J. A., Dentener, F., Ganzeveld, L., and Peters, J. A. H. W.: Recent trends in global greenhouse gas emissions: regional trends and spatial distribution of key sources, in: Non-CO₂ Greenhouse Gases (NCGG-4), edited by: van Amstel, A., Millpress, Rotterdam, 325–330, 2005.

Olivier, J. G. J., Janssens-Maenhout, G., and Peters, J. A. H. W., Trends in global CO₂ emissions, 2012 Report, PBL Netherlands Environmental Assessment Agency, The Hague, Joint Research Centre, Ispra, ISBN 978-92-79-25381-2, 2012.

Oshchepkov, S., A. Bril, T. Yokota, et al., Effects of atmospheric light scattering on spectroscopic observations of greenhouse gases from space. Part 2: Algorithm intercomparison in the GOSAT data processing for CO₂ retrievals over TCCON sites, *J. Geophys. Res.*, 118, 1493–1512, doi:10.1002/jgrd.50146, 2013.

Osterman, G., O'Dell, C., Eldering, A., Fisher, B., Crisp, D., Cheng, C., Frankenberg, C., Lambert, A., Gunson, M., Mandrake, L., & Wunch, D. (2020). Orbiting Carbon Observatory-2 & 3(OCO-2 & OCO-3)—Data product user's guide, operational level 2 data versions 10 and lite file version 10 and VEarly.

	ESA Climate Change Initiative (CCI+) Climate Assessment Report (CAR) for Climate Research Data Package 7 (CRDP#7) of the Essential Climate Variable (ECV) Greenhouse Gases (GHG)	Page 47
		Version 1.1
		20 March 2023

Version 1.0, revision A, 8 June 2020. Pasadena, CA: Jet Propulsion Laboratory. Retrieved from https://docserver.gesdisc.eosdis.nasa.gov/public/project/OCO/OCO2_OCO3_B10_DUG.pdf

Pandey, S., Houweling, S., Krol, M., Aben, I., Chevallier, F., Dlugokencky, E. J., Gatti, L. V., Gloor, M., Miller, J. B., Detmers, R., Machida, T., and Röckmann, T.: Inverse modeling of GOSAT-retrieved ratios of total column CH₄ and CO₂ for 2009 and 2010, *Atmos. Chem. Phys. Discuss.*, doi:10.5194/acp-2016-77, in review, 2016.

Parazoo, N. C., Bowman, K., Frankenberg, C., et al., Interpreting seasonal changes in the carbon balance of southern Amazonia using measurements of XCO₂ and chlorophyll fluorescence from GOSAT, *Geophys. Res. Lett.*, 40, 2829–2833, doi:10.1002/grl.50452, 2013.

Parker, R., Boesch, H., Cogan, A., et al., Methane Observations from the Greenhouse gases Observing SATellite: Comparison to ground-based TCCON data and Model Calculations, *Geophys. Res. Lett.*, doi:10.1029/2011GL047871, 2011.

Peng, S., Lin, X., Thompson, R.L. et al. Wetland emission and atmospheric sink changes explain methane growth in 2020. *Nature* 612, 477–482, doi: 10.1038/s41586-022-05447-w, 2022.

Peters, W., Jacobson, A. R., Sweeney, C., et al.: An atmospheric perspective on North American carbon dioxide exchange: CarbonTracker, *Proceedings of the National Academy of Sciences (PNAS)* of the United States of America, 27 Nov. 2007, 104(48), 18925-18930, 2007.


Peylin, P., Law, R. M., Gurney, et al., Global atmospheric carbon budget: results from an ensemble of atmospheric CO₂ inversions, *Biogeosciences*, 10, 6699–6720, doi:10.5194/bg-10-6699-2013, URL <http://www.biogeosciences.net/10/6699/2013/>, 2013.

Pinty, B., G. Janssens-Maenhout, M. Dowell, H. Zunker, T. Brunhes, P. Ciais, D. Dee, H. Denier van der Gon, H. Dolman, M. Drinkwater, R. Engelen, M. Heimann, K. Holmlund, R. Husband, A. Kentarchos, Y. Meijer, P. Palmer and M. Scholze (2017) An operational anthropogenic CO₂ emissions monitoring & verification support capacity - Baseline requirements, Model components and functional architecture, doi:10.2760/39384, European Commission Joint Research Centre, EUR 28736 EN.

Poulter, B., Frank, D., Ciais, P., Myneni, R. B., Andela, N., Bi, J., Broquet, G. Canadell, J.G. Chevallier, F. Liu, Y. Y., Running, S. W., Sitch, S., and van der Werf, G. R.: Contribution of semi-arid ecosystems to interannual variability of the global carbon cycle. *Nature*, doi:10.1038/nature13376, 2014.

Prather, M.: Interactive comment on “Carbon dioxide and climate impulse response functions for the computation of greenhouse gas metrics: a multi-model analysis” by F. Joos et al, *Atmos. Chem. Phys. Discuss.*, 12, C8465–C8470, www.atmos-chem-phys-discuss.net/12/C8465/2012/, 2012.

Remaud, M., Chevallier, F., Cozic, A., Lin, X., and Bousquet, P.: On the impact of recent developments of the LMDz atmospheric general circulation model on the simulation of CO₂ transport, *Geosci. Model Dev.*, 11, 4489–4513, <https://doi.org/10.5194/gmd-11-4489-2018>, 2018.

	ESA Climate Change Initiative (CCI+)		Page 48
	Climate Assessment Report (CAR) for Climate Research Data Package 7 (CRDP#7)		Version 1.1
			20 March 2023
	of the Essential Climate Variable (ECV) Greenhouse Gases (GHG)		

Reuter, M., Bovensmann, H., Buchwitz, M., et al., Retrieval of atmospheric CO₂ with enhanced accuracy and precision from SCIAMACHY: Validation with FTS measurements and comparison with model results, *J. Geophys. Res.*, 116, D04301, doi:10.1029/2010JD015047, 2011.

Reuter, M., Boesch, H., Bovensmann, H., et al., A joint effort to deliver satellite retrieved atmospheric CO₂ concentrations for surface flux inversions: the ensemble median algorithm EMMA, *Atmos. Chem. Phys.*, 13, 1771-1780, 2013.

Reuter, M., M. Buchwitz, M. Hilker, et al., Satellite-inferred European carbon sink larger than expected, *Atmos. Chem. Phys.*, 14, 13739-13753, doi:10.5194/acp-14-13739-2014, 2014a.

Reuter, M., M. Buchwitz, A. Hilboll, et al., Decreasing emissions of NO_x relative to CO₂ in East Asia inferred from satellite observations, *Nature Geoscience*, 28 Sept. 2014, doi:10.1038/ngeo2257, pp.4, 2014b.

Reuter, M.: ESA Climate Change Initiative (CCI) Product User Guide version 4 (PUGv4) for the XCO₂ SCIAMACHY Data Product BESD for the Essential Climate Variable (ECV): Greenhouse Gases (GHG), 31 August 2016, 2016a.


Reuter, M., M. Hilker, O. Schneising, M. Buchwitz, J. Heymann ESA Climate Change Initiative (CCI) Comprehensive Error Characterisation Report: BESD full-physics retrieval algorithm for XCO₂ for the Essential Climate Variable (ECV) Greenhouse Gases (GHG) Version 2.0, revision 1. 2016b.

Reuter, M., M. Buchwitz, M. Hilker, J. Heymann, H. Bovensmann, J. P. Burrows, S. Houweling, Y. Y. Liu, R. Nassar, F. Chevallier, et al., How much CO₂ is taken up by the European terrestrial biosphere?, *Bulletin of the American Meteorological Society*, 0(0), doi:10.1175/BAMS-D-15-00310.1, 2016c.

Reuter, M., M. Buchwitz, O. Schneising, S. Noel, V. Rozanov, H. Bovensmann, J. P. Burrows, A Fast Atmospheric Trace Gas Retrieval for Hyperspectral Instruments Approximating Multiple Scattering - Part 1: Radiative Transfer and a Potential OCO-2 XCO₂ Retrieval Setup, *Remote Sens.*, 9, 1159, doi:10.3390/rs9111159, 2017a.

Reuter, M., M. Buchwitz, O. Schneising, S. Noel, H. Bovensmann, J. P. Burrows, A Fast Atmospheric Trace Gas Retrieval for Hyperspectral Instruments Approximating Multiple Scattering - Part 2: Application to XCO₂ Retrievals from OCO-2, *Remote Sens.*, 9, 1102, doi:10.3390/rs9111102, 2017b.

Reuter, M., Buchwitz, M., Schneising, O., Noël, S., Bovensmann, H., Burrows, J. P., Boesch, H., Di Noia, A., Anand, J., Parker, R. J., Somkuti, P., Wu, L., Hasekamp, O. P., Aben, I., Kuze, A., Suto, H., Shiomi, K., Yoshida, Y., Morino, I., Crisp, D., O'Dell, C. W., Notholt, J., Petri, C., Warneke, T., Velasco, V. A., Deutscher, N. M., Griffith, D. W. T., Kivi, R., Pollard, D. F., Hase, F., Sussmann, R., Té, Y. V., Strong, K., Roche, S., Sha, M. K., De Mazière, M., Feist, D. G., Iraci, L. T., Roehl, C. M., Retscher, C., and Schepers, D.: Ensemble-based satellite-derived carbon dioxide and methane column-averaged dry-air mole fraction data sets (2003–2018) for carbon and climate applications, *Atmos. Meas. Tech.*, 13, 789–819, <https://doi.org/10.5194/amt-13-789-2020>, 2020.

	ESA Climate Change Initiative (CCI+)		Page 49
	Climate Assessment Report (CAR) for Climate Research Data Package 7 (CRDP#7)		Version 1.1
			20 March 2023
	of the Essential Climate Variable (ECV) Greenhouse Gases (GHG)		

Rödenbeck, C.: Estimating CO₂ sources and sinks from atmospheric mixing ratio measurements using a global inversion of atmospheric transport, Tech. Rep. 6, Max Planck Institute for Biogeochemistry, Jena, Germany, 2005.

Ross, A. N., Wooster, M. J., Boesch, H., Parker, R., First satellite measurements of carbon dioxide and methane emission ratios in wildfire plumes, *Geophys. Res. Lett.*, 40, 1-5, doi:10.1002/grl.50733, 2013.

Scarcle, J. D., Studies in astronomical time series analysis. III. Fourier transforms, autocorrelation functions and cross-correlation functions of unevenly spaced data. *Astrophys. J.*, 343, 874–887, 1989.

Schneising, O., Buchwitz, M., Reuter, M., et al., Long-term analysis of carbon dioxide and methane column-averaged mole fractions retrieved from SCIAMACHY, *Atmos. Chem. Phys.*, 11, 2881-2892, 2011.

Schneising, O., J. Heymann, M. Buchwitz, M. Reuter, H. Bovensmann, and J. P. Burrows, Anthropogenic carbon dioxide source areas observed from space: assessment of regional enhancements and trends, *Atmos. Chem. Phys.*, 13, 2445-2454, 2013.


Schneising, O., M. Reuter, M. Buchwitz, J. Heymann, H. Bovensmann, and J. P. Burrows, Terrestrial carbon sink observed from space: variation of growth rates and seasonal cycle amplitudes in response to interannual surface temperature variability, *Atmos. Chem. Phys.*, 14, 133-141, 2014a.

Schneising, O., J. P. Burrows, R. R. Dickerson, M. Buchwitz, M. Reuter, H. Bovensmann, Remote sensing of fugitive methane emissions from oil and gas production in North American tight geologic formations, *Earth's Future*, 2, DOI: 10.1002/2014EF000265, pp. 11, 2014b.

Schneising, O., Buchwitz, M., Reuter, M., Bovensmann, H., Burrows, J. P., Borsdorff, T., Deutscher, N. M., Feist, D. G., Griffith, D. W. T., Hase, F., Hermans, C., Iraci, L. T., Kivi, R., Landgraf, J., Morino, I., Notholt, J., Petri, C., Pollard, D. F., Roche, S., Shiomi, K., Strong, K., Sussmann, R., Velasco, V. A., Warneke, T., and Wunch, D.: A scientific algorithm to simultaneously retrieve carbon monoxide and methane from TROPOMI onboard Sentinel-5 Precursor, *Atmos. Meas. Tech.*, 12, 6771–6802, <https://doi.org/10.5194/amt-12-6771-2019>, 2019.

Schneising, O., Buchwitz, M., Reuter, M., Bovensmann, H., and Burrows, J. P.: Severe Californian wildfires in November 2018 observed from space: the carbon monoxide perspective, *Atmos. Chem. Phys.*, 20, 3317–3332, <https://doi.org/10.5194/acp-20-3317-2020>, 2020.

Schulze, E. D., Luyssaert, S., Ciais, P., Freibauer, A., Janssens, I. A., Soussana, J. F., Smith, P., Grace, J., Levin, I., Tiruchittampalam, B., Heimann, M., Dolman, A. J., Valentini, R., Bousquet, P., Peylin, P., Peters, W., Rodenbeck, C., Etiope, G., Vuichard, N., Wattenbach, M., Nabuurs, G. J., Poussi, Z., Nieschulze, J., Gash, J. H., and Team, C.: Importance of methane and nitrous oxide emissions for Europe's terrestrial greenhouse gas balance, *Nat. Geosci.*, 2, 842–850, 2009.

	ESA Climate Change Initiative (CCI+)		Page 50
	Climate Assessment Report (CAR)		
	for Climate Research Data Package 7 (CRDP#7)		Version 1.1
	of the Essential Climate Variable (ECV) Greenhouse Gases (GHG)		20 March 2023

Shindell, D. T., O. Pechony, A. Voulgarakis, et al., Interactive ozone and methane chemistry in GISS-E2 historical and future climate simulations, *Atmos. Chem. Phys.*, 13, 2653–2689, doi:10.5194/acp-13-2653-2013, 2013.

Somkuti, P.: ESA Climate Change Initiative (CCI) Product User Guide version 4.0 (PUGv4.0) for the University of Leicester full-physics XCO₂ GOSAT data product (CO2_GOS_OCFP version 7) for the Essential Climate Variable (ECV): Greenhouse Gases (GHG), 31 August 2016, 2016.

Sussmann, R., Forster, F., Rettinger, M., and Bousquet, P.: Renewed methane increase for five years (2007–2011) observed by solar FTIR spectrometry, *Atmos. Chem. Phys.*, 12, 4885–4891, doi:10.5194/acp-12-4885-2012, 2012.

Turner, A. J., Jacob, D. J., Wecht, K. J., Maasakkers, J. D., Lundgren, E., Andrews, A. E., Biraud, S. C., Boesch, H., Bowman, K. W., Deutscher, N. M., Dubey, M. K., Griffith, D. W. T., Hase, F., Kuze, A., Notholt, J., Ohyama, H., Parker, R., Payne, V. H., Sussmann, R., Sweeney, C., Velasco, V. A., Warneke, T., Wennberg, P. O., and Wunch, D.: Estimating global and North American methane emissions with high spatial resolution using GOSAT satellite data, *Atmos. Chem. Phys.*, 15, 7049–7069, doi:10.5194/acp-15-7049-2015, 2015.

Wanninkhof, R., Park, G. -H., Takahashi, T., Sweeney, C., Feely, R., Nojiri, Y., Gruber, N., Doney, S. C., McKinley, G. A., Lenton, A., Le Quéré, C., Heinze, C., Schwinger, J., Graven, H., and Khatiwala, S.: Global ocean carbon uptake: magnitude, variability and trends, *Biogeosciences*, 10, 1983–2000, doi:10.5194/bg-10-1983-2013, 2013.


van der Werf, G. R., Randerson, J. T., Giglio, L., Collatz, G. J., Mu, M., Kasibhatla, P. S., Morton, D. C., DeFries, R. S., Jin, Y., and van Leeuwen, T. T.: Global fire emissions and the contribution of deforestation, savanna, forest, agricultural, and peat fires (1997–2009), *Atmos. Chem. Phys.*, 10, 11707–11735, doi:10.5194/acp-10-11707-2010, 2010.

Wecht, K. J., D. J. Jacob, C. Frankenberg, Z. Jiang, and D. R. Blake (2014), Mapping of North American methane emissions with high spatial resolution by inversion of SCIAMACHY satellite data, *J. Geophys. Res. Atmos.*, 119, 7741–7756, doi:10.1002/2014JD021551.

Wunch, D., Toon, G. C., Blavier, J.-F., et al., The Total Carbon Column Observing Network, *Phil. Trans. R. Soc. A*, 369, 2087–2112, doi:10.1098/rsta.2010.0240, 2011.

Wunch, D., Wennberg, P. O., Toon, G. C. et al., A method for evaluating bias in global measurements of CO₂ total columns from space. *Atmos. Chem. Phys.*, 11, 12317–12337, 2011.

Yang, D. X., and Coauthors, 2021: A new TanSat XCO₂ global product towards climate studies. *Adv. Atmos. Sci.*, 38(1), 8–11, <https://doi.org/10.1007/s00376-020-0297-y>.

	ESA Climate Change Initiative (CCI+)		Page 51
	Climate Assessment Report (CAR) for Climate Research Data Package 7 (CRDP#7)		
			Version 1.1
	of the Essential Climate Variable (ECV) Greenhouse Gases (GHG)		20 March 2023

Yoshida, Y., Kikuchi, N., Morino, I., et al., Improvement of the retrieval algorithm for GOSAT SWIR XCO₂ and XCH₄ and their validation using TCCON data, *Atmos. Meas. Tech.*, 6, 1533–1547, doi:10.5194/amt-6-1533-2013, 2013.

END OF DOCUMENT